

## Chapter 2

# Natural Rubber Nanoblends: Preparation, Characterization and Applications

Oriparambil Sivaraman Nirmal Ghosh, S. Gayathri,  
P. Sudhakara, S.K. Misra and J. Jayaramudu

**Abstract** Natural rubber nanocomposites are emerging as one of the key players in the industry and research due to its novel material properties and nanofunctionalities. The development of nanotechnology provided a wide range of methods for the synthesis of novel multifunctional nanofillers and blending them with natural rubber to make high performance natural rubber nanocomposites. In this chapter we summarize the advanced methods for synthesis, characterization and applications of natural rubber nanoblends using various techniques including skim latex mixing, latex/melt intercalation, freeze drying and in-situ non-aqueous sol-gel method. A detailed description of advanced nanomaterial characterization methods like XRD, XPS, XRF, UV-Vis spectroscopy, Photoluminescence spectroscopy, Raman spectroscopy, TGA-DTA, SEM-EDX, EPMA, TEM-SAED, VSM and FTIR are also elaborated for understanding the physicochemical characteristics of nanofillers and natural rubber nanocomposites. A brief outline of current trends in the development of nanomaterials for filler applications was summarized. The fundamental aspects of design and utilization of various nanostructured materials including carbon nanotubes, clay, iron oxide, zinc oxide, nickel, silica, gold, silver and graphene based filler materials are discussed in detail.

**Keywords** Natural rubber · Nanoblend · Nanocomposite · Nanofiller · Advanced characterization technique

---

O.S. Nirmal Ghosh (✉) · S. Gayathri  
Nanophotonics and Nanoelectronics Research Laboratory, Centre for Nanoscience and Technology, Madanjeet School of Green Energy Technologies, Pondicherry University, Kalapet 605014, India  
e-mail: nirmalgvr@protonmail.ch

P. Sudhakara · S.K. Misra  
Regional Centre for Extension and Development, CSIR—Central Leather Research Institute, Leather Complex, Jalandhar 144021, Punjab, India

J. Jayaramudu  
Indian Rubber Manufacturers Research Association, Thane 400604, Maharashtra, India

## 2.1 Introduction

Natural rubber (NR) is an elastomer which is derived from a milky colloidal suspension from the sap of typical plants. The chemical structure of the NR is given in Fig. 2.1. NR is generally known as *cis*-1,4-poly (isoprene). *Hevea brasiliensis* plant is originated from Brazil. Among the rubber plants, the *Hevea brasiliensis* is the only sap tree having commercial and industrial significance. *Hevea* trees are the natural source with high molecular weight approximately 97 % *cis*-1,4-poly (isoprene), and due to this high molecular weight, the NR polymer chain continues to be on the same side of the double bond. Due to its regularity of the structure, the NR undergoes crystallization when it is stored below 20 °C or subject to stretching. The specific gravity of NR is 0.93 at 20 °C.

*Hevea* trees produce high-yield latex for a tapping period of 30 years. The NR latex contains 60 % water, 36 % of total solid content, 33 % dry rubber content, 1–2.5 % of proteinaceous substances, 1–2.5 % of resinous substance, 1 % sugar, less than 1 % ash, and 0.5 % of salts of phosphorus, potassium, and magnesium. Due to the sticky and unsaturated bonding nature of NR, it does not have any industrial significance up to 1839 (Fig. 2.2).

In 1839, Thomas Hancock and Charles Goodyear have independently invented vulcanization process to chemically modify the NR and establish cross-links into the NR chains. The vulcanization process is a systematic process of converting the NR into a non-sticky and hard polymeric material by adding sulfur, accelerators, antioxidants, and fillers. It is an irreversible chemical process. The mechanical

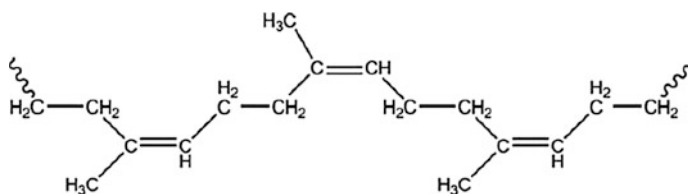
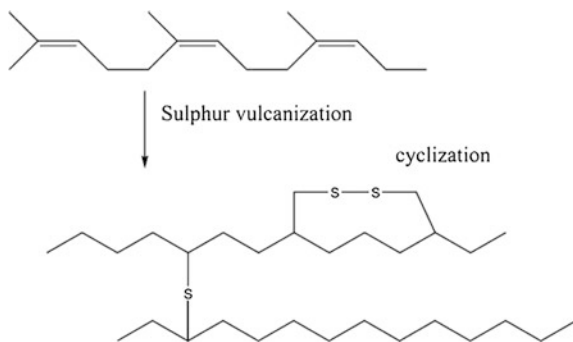


**Fig. 2.1** Chemical structure of natural rubber (*cis*-1,4-poly(isoprene))

**Fig. 2.2** Schematic of sulfur vulcanization of natural rubber



properties of the NR increase during the vulcanization process due to the cross-linking of NR chains. The vulcanized rubbers have very high resistance to organic solvents with improved elastic and flexible nature. During the advanced vulcanization process, NR is compounded with different concentrations of fillers, low concentration of accelerators, aromatic amines, and phenols for antioxidation purposes and 5–8 % of sulfur followed by the temperature treatment. Natural rubber nanocomposites (NRNs) are having wide range of applications in the field of industry and technology. NRNs containing required amount of Montmorillonite structures composed of nanostructured alumino-silicate layers which acts as filler to reinforce the NR matrix. As a result of this clay-based filler reinforcement, the water permeability of NR decreases considerably with simultaneous enhancement in superior thermal and mechanical properties. Dynamic vulcanization techniques are used to manufacture NR-based polymer blends. Therefore, through this method, it is possible to develop high-performance thermoplastics with improved mechanical and thermal properties with low hardness [1].

Nanoscience and technology deals with the development of nanomaterials and studying its characteristics for various applications. The rise of the nanoera in science and technology also has great impact in the development of rubber technology. Generally, nanomaterials have low-dimensional aspects and size varying from 1 to 100 nm. All the electrons present in the nanomaterials are available on the surface due to its high surface to volume ratio. A wide range of multifunctional nanomaterials are used as fillers and antioxidation agents to enhance the mechanical, thermal, electrical, and magnetic properties of the NR. The nanofillers act as the major reinforcement agent in NR matrix. It is found that the fillers help to enhance the tensile strength, tear resistance, aberration resistance, and tensile modulus of the NR. The physicochemical and mechanical properties of NR are closely related with that of filler materials used. Utilization of nanostructured materials as fillers leads to the development of NRNs and nanotechnology revolution in rubber technology. The performance of filler in the NR matrix is governed by the surface interface characteristics which include concentration, particle size, shape, structure, and degree of interactions with rubber matrix and surface of the particle agglomerates. Compared to the bulk filler materials, nanostructured filler materials exhibit special properties such as high surface area, mechanical strength, wear, tear and aberration resistance, antioxidation properties, control over dimensions, and electronic confinement. Due to the large surface area of nanomaterials, higher level of surface interface interaction between rubber matrix and nanofillers is possible in NRNs. The formation of surface interface between NR and nanofillers is governed by the volume fraction and size of the constituent nanoparticles. The degree of bonding between NR matrix and nanofiller particles is the major influencing factor in determining the degree of reinforcement in elastomer properties of NRN.

A NRN is a multiphase solid material where one of the phases has dimension below the range of 100 nm. During the synthesis of NRN, the nanofillers are added into the natural rubber at rates from 1 % to 10 wt%. The nanofillers are categorized into various types according to the nanodimension and behavior of the fillers. Generally, one-dimensional nanofillers are in the form of laminas, shells, and plates.

Nanotubes and fibers with diameter lesser than 100 nm are considered as two-dimensional nanofillers. The template like isodimensional nanostructured materials is considered as three-dimensional nanofillers. Due to the importance and advantages of nanostructured materials in NRN, scientific communities across the globe are attracted very much toward the emerging field of research in NRN and various techniques for the production and characterization of NRN. In this regard, we tried to summarize the current literature available in the field of NRN research in this chapter. The fundamental aspects of physicochemical characterization of NRN and nanostructured materials are also included and discussed in this chapter for the benefit of scientists and beginners in NRN research.

## 2.2 Recent Works on Natural Rubber Blends

Due to the wide attention given to the natural rubber blends, a lot of literatures have been evolved in past few years. Scientists from various fields are working together on developing high-performance natural rubber composites for different industrial applications. Recent development in the field of nanotechnology research provided a boost up in the development of NRNs. Development and utilization of nanofillers and functional additives as reinforcement materials helps to provide nanofunctionalities to the NRN that includes high mechanical stability, aberration resistance, resistance against organic liquids and solvents, and enhanced thermal stability. Thus, the novel properties of the nanomaterials can be extended to its natural rubber composites also. J. Wu et al. recently demonstrated the enhancement in vulcanization kinetics of NRN through the addition of graphene during the vulcanization process. In a typical synthesis process, they have mixed the graphene efficiently with the NR to reduce the induction period of vulcanization process. It is identified that upon addition of graphene the induction period was suddenly suppressed. They recognized that the graphene loading has influence in vulcanization kinetics in such a way that the low graphene loading enhances the vulcanization kinetics, and upon increasing the graphene loading, there is a slight increase in induction period of vulcanization process. They found that the graphene reduces the melting point of sulfur and provides enhancement in cross-linking of NR. This enhanced cross-linking results an increase in cross-linking density of graphene NRN. It is identified that the addition of graphene leads to the accelerated reaction between accelerator, sulfur, and activator [2]. In the similar fashion, G. Sui et al. explored the ability of carbon nanotubes as a reinforcement agent [3]. In this extensive study, Sui group used the pretreated CNT as fillers to improve the dynamic compression properties, thermal stability, rebound resilience, and storage modulus of the NRN. The CNTs were prepared using chemical vapor deposition (CVD) followed by purification in hydrofluoric acid (HF) for 24 h and washed continuously by using deionized water until the pH become neutral. Further, they have adopted a typical treatment method to improve the reinforcement through better cross-linking of fillers and NR matrix. CNT-NRN was prepared by solvent mixing and two-roll

milling. Interesting observations have been made in this study proves that the utilization of pretreated CNT as a filler in NR helps to improve the mechanical properties. This is due to the high surface to volume ratio of CNT and formation of better coordination bonding between NR matrix and CNT [3].

Fine-tuning the electrical and mechanical properties of NRN is taking great importance due to wide range of applications in energy storage devices, sensors, etc. International scientist community have paid lot of attention to this area to develop novel nanoblend-based NRN. Recently, Thomas et al. demonstrated the effect of functionalized CNTs in enhancement of electrical properties of NRN. They have found that the dielectric constant of the NRN increases with increase in CNT loading. 1-octadecanol was used to modify the CNT for better dispersibility. It is found that the 1-octadecanol-functionalized CNT fillers show better stress transfer from NR matrix to the filler. Due to this reason, the fillers tensile strength and elongation at break of the NRN with functionalized CNT was better than that of NRN with normal CNT as fillers [4]. Efforts have been made to manipulate the thermal properties of NR using graft copolymerization techniques. Recently, Nakason et al. was successfully achieved the copolymerization of maleic anhydride and NR to improve the glass transition temperature of the graft copolymers of NR and anhydride [5]. Dispersion of fillers in the NR matrix is a very important factor which influences the mechanical, thermal, and electrical properties of NRN. Multiwall carbon nanotubes (MWCNTs) are one of the key players as fillers which not only reinforce the NR but also it facilitate improvement in stiffness of the NR matrix. Bokobza et al. found that the good dispersion of MWCNTs leads to the formation of NRN with high electrical and mechanical properties. According to Halpin-Tsai model, the aspect ratio of the MWCNTs should be 90 in order to achieve an optimal dispersion of MWCNTs in NR matrix to form a NRN with superior material properties such as electrical conduction and mechanical reinforcement [6].

Nanostructured fillers and curing agents are attracting enormous attention due to the environmental concerns and health issues related to the conventional chemicals. Nanofillers, antioxidants, and curing agents have unique properties of high surface to volume ratio due to their nanosize and shape. This will help the NR industry to meet out the large requirement of chemicals for NR production and manufacturing. Using the nanoadditives which help us to reduce the consumption of chemicals, since they provide the same performance at low weight percentage compared to the bulk counter parts. In this regard, Kim et al. conducted an exclusive investigation to understand the effect of nanostructured ZnO on the mechanical properties and cure characteristics of silica-filled NRNs. In this study, they have used nano-ZnO with particle size varies in the range of 30–40 nm and specific surface area of 25–50 m<sup>2</sup>/gm. In contrary to the conventional volume of bulk ZnO, they have added only 20 wt% nano-ZnO into the unfilled system and achieved the same level of cure characteristics and mechanical properties achieved by adding higher volume of bulk ZnO. This is due to the large specific surface area of nano-ZnO, which led to the increase in the degree of cross-linking in NR matrix [7]. Nanofibers are also used as reinforcing agents in NR. Nanofibers of cellulose generated from biological

resources like plants are having important role in providing alternate resources for the manufacturing of green NRN. This approach provides an economically viable method to enhance the mechanical and loadbearing properties of NRN. Recently, Abraham et al. was reported the fabrication of NRN using cellulose nanofiber and natural rubber latex. In this work, the researchers have isolated cellulose nanofibers (CNF) from raw banana fibers by steam explosion process. The CNF-based NRN exhibits improved Young's modulus and tensile strength. Dynamic mechanical analysis showed that with the addition of CNF in NR there is a considerable change in the storage modulus of the NR matrix. This is due to the reinforcement effect of CNF in the NR latex [8].

In a similar study carried out by Bendahou et al., cellulose whiskers and microfibrillated cellulose were extracted from the rachis of the palm from *Phoenix dactylifera* L as a reinforcement agent in natural rubber matrix, and they have found that the swelling behavior of NRN by toluene was decreasing considerably with the addition of only 1 wt% of cellulose in NR matrix. From their results, it is obtained that the higher filler–matrix interaction and adhesion modify the physicochemical properties of the NRN. Compared to NR, the cellulose-NR composites exhibit enhanced material properties including high stiffness, low shrinkage and reduced water intake. The addition of cellulose whiskers created an interfacial layer surrounding the filler which restricts the mobility of fillers in NR matrix resulting better mechanical properties compared to its bulk counterparts [1]. Making of blends NR with polymers like acrylonitrile butadiene rubber (NBR) is an easiest way to achieve better thermal stability. Kumari et al. reported that blending of NBR with NR helps to increase the decomposition temperature of NR–NBR composite, which is due to the enhancement in interfacial adhesion between the NR and NBR blend components. Also they have observed that the addition of compatibilizer like neoprene does not affect the thermal stability of the blends, and NR–NBR blends are thermodynamically immiscible even after addition of compatibilizer [9]. Fillers are widely used to reinforce the natural rubber matrix and make the NR suitable for real time applications by uplifting its performance. The nanostructural properties of fillers have a great influence over the linear viscoelastic properties. Recently, Zachariah et al. reported the rheological properties of NR–clay nanocomposite (NRCN) in which the organoclay nanomer 1.44P was treated with surfactant containing hydrogenated tallow, quaternary ammonium. It revealed that the viscosity of the NRCN is directly proportional to the nanofiller component in the NRCN [10].

Due to the development in design and product development, there is a huge demand for elastomer-based novel nanocomposites for flexible electronics and electrical industry. Metallic nanoparticle-dispersed flexible elastomers are of particular interest due to their semiconducting and nanofunctional properties. The insulating properties of natural elastomer were modified by tuning the dielectric properties by impregnating the nickel nanoparticles in NR matrix. This method provides a novel approach in changing the magnetic as well as electrical properties of NR to incorporate the desired physicochemical properties matching for technological applications. There is an appreciable change in elastic modulus of the NRN with the increase in nickel metallic nanoparticle-based filler concentration.

The synthesized NRN showed ferromagnetic behavior which can be attributed to the characteristic contribution from the magnetic property of nickel nanoparticles incorporated in the NR matrix [11]. Current advancements in nanomaterials opened a bright corridor in ultrasensitive membrane-based sensors, actuators, and transducers. The size tunable photoluminescent properties of nanomaterials make them amicable for developing sensors. The surface plasmon resonance properties and band gap confinement of metal nanoparticles such as gold and silver have potential applications in development of metal nanoparticle–NR nanocomposites for ultrathin membranes for nanosensors. Recently, Cabrera et al. reported the fabrication of NR–Au nanoparticle-based membranes for optical sensing. The gold nanoparticles show a tendency to agglomerate together during interaction with organic acids and proteins, which leads to the optical quenching in photoluminescence due to the increase in band gap resulted from the increase in nanocluster size. They had fabricated a NR membrane by casting method, and gold nanoparticle was incorporated through a facile direct reduction of Au(III) in the NR membrane itself. The casted NR membrane was dipped into a solution containing gold precursor, and the solvated gold ions are reduced by the constituent organic acids and proteins present in the NR membrane. The reduced gold nanoparticles formed on the NR membrane surface attributes novel photoluminescence functionalities with in the sensible range suitable for the development of nanosensors [12]. In a similar fashion, silver–NR nanocomposites were prepared by reduction of silver salt followed by UV light exposure. This method provides an economical way of preparing Ag–NR nanocomposites for antibacterial, electrical, thermal, and optical applications [13]. Zakaria et al. observed that the NR matrix reinforced with alumina boron carbide nanofillers shows excellent mechanical properties due to the high surface energy of the filler particles. While keeping the electrical insulation properties in its lower limits, the thermal conductivities of aluminum oxide and boron carbide provide superior heat transfer ability to the NRN and make them highly desirable for high-temperature electrical insulation purposes [14]. High-performance-grade fluoroelastomer rubber (FR) is usually used for applications in automotive, aerospace, and petrochemical industries. The FR usually consists of vinylidene fluoride (VDF), which facilitates the increase in bond dissociation energy of the C–F bond present in the FR. Due to this, the fluoroelastomers have long-lasting specific resistance to oil and chemicals at high temperature (200 °C). Due to this, high thermal stability and resistance against chemical degradation, FR is widely used in O-rings, hoses and seals. FR-blended NRNs along with nanofillers have particular interest due to their good interfacial bonding, elongation at break values, enhanced thermal and mechanical stability at vigorous performing conditions [15]. Latest development in the NRN-based soft electromechanical generators for sustainable energy development provides an economically viable way for power production. This novel approach can help us to partially meet out the huge energy demand in the current scenario through the utilization of sustainable energy resources like ocean energy [16].

Quitmann et al. observed that constrained shape memory natural rubber (SMNR) acts as stress generator upon the exposure of selected solvent vapor and regains

their shape after removing the solvent exposure. The stress generated during the exposure of solvent vapor is proportional to the concentration of the solvent vapor and also this process is reversible. These peculiarities made them an interesting candidate for wide range of applications in elastomers for shape memory applications [17]. Development of novel NRN for applications in petrochemical industry has particular interest due to the key role of these materials in hydrocarbon transport, storage, and supply systems. Raghavachari et al. observed that the NRN can be used as good alternative for oil spill recovery. The environmental pollution caused by the oil spill from crude carriers and oil wells in sea is projecting great threat to the marine ecosystem and sustainable habitat of rare marine species. In this regard, they have used nanocomposites of epoxidized natural rubber with magnetite for adsorbing petrol and recovering it [18]. New approaches in dynamic vulcanization techniques resulted in the formation of supertoughened NRN have great industrial importance. Chen et al. reported the development of biobased polyactide/NRN with continuous cross-linked phase through a facile dynamic vulcanization method. Their research group demonstrated the fabrication of ultra-toughened PLA/NRN with continuously cross-linked network of NR. The enhancement in interfacial compatibilization resulted from the PLA grafting onto NR was the major reason for supertoughness of the developed NRN [19].

Great efforts are there to replace the synthetic polymers with their biobased counterparts. Mohanty et al. demonstrated the fabrication of NRN of polyhydroxybutyrate (PHB) blended with epoxidized NR and maleated polybutadiene. This revolutionary approach will be very helpful in the development of biodegradable toughened bacterial polyester of epoxidized NR. The developed NRN can be used as environmental friendly and alternative for non-degradable polyolefins that facilitate the remediation of pollution caused by the deposition of synthetic polymers derived from hydrocarbons [20]. Nowadays, lightweight, flexible, and environment-friendly electromagnetic wave absorbing elastomers are attracting enormous attention due to the spiking demand of such materials in applications in aerospace engineering, telecommunication devices, electrical components, electronic gadgets, and machineries for biomedical and military applications. Kong et al. observed that the nanocomposites of iron oxide with NR can be used as microwave absorbing material [21]. Physicochemical and mechanical properties of the NRN can be modified by using organoclay fillers. Intercalation functionalities of these organoclay fillers can be modified by organic functionalization using alkyl functional groups with varying chain length. It is observed that the cross-linking density of NR was drastically improved by using organoclay fillers containing alkylammonium groups. The dispersion of clay fillers in NR matrix and vulcanization reaction of NR was accountably increased due to the organic functional modification of clay fillers [22]. NRNs of graphene is one of the hottest areas of NRN due to the attractive material properties of graphene. The exfoliated layers of graphite provide great interaction between the filler and NR matrix, which improves the mechanical properties to a great extent. The special electrical properties of graphene also provide electrical and conducting properties to the graphene-based NRNs [23]. Reduced graphene oxide (RGO) particles are also widely used as filler

material to enhance the thermal, mechanical, and electrical properties of NR composites. Ruoff et al. observed that cocoagulation of RGO and NR generates web-like surface morphology due to the interaction of RGO flakes with latex particles. As a result of incorporation of RGO in NR matrix, the conductivity and stiffness of the RGO NRN were greatly increased. The conducting elastomers have potential upthrust in flexible electronics industry upsurges the utilization of graphene like nanomaterials in the development of NRN [24]. In the near future, the rapid advancements in nanotechnology will lay down the stepping stones for the development of smart and intelligent NRNs for functional applications in unconventional areas in science and technology.

## 2.3 Preparation of Natural Rubber Nanoblends

### 2.3.1 Skim Latex Mixing

In the skim latex mixing process, the natural latex rubber is centrifuged to obtain the protein rich by product called as skim natural rubber latex. This skim natural latex rubber is treated with surfactant and alkali to remove the aqueous phase by forming the creamy skim latex. The nanofillers are added into this creamy skim latex and mixed well followed by the addition of formic acid to initiate the coagulation process and obtain a consolidated mass, followed by drying and vulcanization process to obtain the NRN. Rosamma Alex et al. reported the preparation of NRNs using organoclay nanofillers using skim latex mixing. They reported that in a typical procedure the skim latex, surfactant, and alkali are mixed together at a fixed concentration and definite time to initiate the protein hydrolysis, which produces the polypeptides and amino acids. Also during the skim latex mixing process, the surfactant is adsorbed over the rubber particles formed which lead to the creaming of natural rubber latex. The aqueous serum layer formed was removed by filtration. The nano-organoclay-based fillers are dispersed in water and mixed with the creamed skim latex followed by mechanical stirring. The serum formed during this process was removed, and reaction temperature was maintained at 35 °C constantly throughout the process. After thorough mixing of nanostructured organoclay fillers, required amount of formic acid is added into the reaction mixture to coagulate the skim latex and obtain the organoclay-filled coagulum. Further, the obtained coagulate was washed with distilled water to remove the remaining acid content completely. The coagulum was then processed by drying in an air oven at 70 °C for 24 h and the dried rubber had a pale yellow color. This dried rubber was mixed with the required compounding ingredients including zinc oxide, stearic acid, polymerized 2,2,4-trimethyl-1,2-dihydroquinoline, *N*-cyclohexy-2-benzothiazole sulfenamide, and sulfur. After proper mixing, the obtained compound was vulcanized at 150 °C to their optimum cure time using a hydraulic press having electrical heating setup to heat the operating metal plates for providing the fixed heat of 150 °C to vulcanize the compounded rubber nanocomposite [25].

### 2.3.2 *Latex/Melt Intercalation Method*

The latex/melt intercalation method is used to prepare the multicomponent rubber nanocomposite blends. In this process, first, the required nanofillers are dispersed in distilled water to form an aqueous dispersion of the nanofillers. Further, the natural rubber latex was mixed with this nanofiller aqueous solution and stirred well. Then, the required amount of acid is added into the above obtained mixture to coagulate the consolidated solid mass of rubber particles mixed with nanofillers. The obtained compound was washed with distilled water to remove the acid content thoroughly followed by heating at 80 °C for 24 h under reduced pressure to obtain the NRN. The polymer which is to be blended with the natural rubber was mixed thoroughly with pure natural rubber and this compound was mixed with the already prepared natural rubber mixed with nanofillers. Thus, the two compounds are mixed together and compounded with other required compounding ingredients at 60–70 °C followed by the addition of accelerator, sulfur, and antioxidant. The obtained rubber compound was vulcanized at 150 °C for the optimum cure time ( $t_{90}$ ) determined by an oscillating disk rheometer. The vulcanization and compounding processes were carried out using a hydraulic press with electrical heating plates kept at a constant temperature of 150 °C.

Recently, Mahdi Abdollahi et al. reported the preparation of natural rubber/butadiene rubber (NR/BR) blend/sodium-montmorillonite nanocomposites by combined latex/melt intercalation method. In a typical process, they have prepared the clay nanocomposites of NR/BR blend. 75 wt% of natural rubber was mixed with the 2 wt% aqueous solution of montmorillonite clay by using latex mixing method. The obtained natural rubber latex/nanofiller solution was coagulated by adding required amount of sulfuric acid and washed several time to remove the remaining acid content. The coagulum was further heated at 80 °C for 24 h under reduced pressure. Simultaneously, the BR was mixed with NR in a 6-in. two-roll mill. In a typical preparation method to make NR/BR/clay nanocomposites, firstly, NR and NR/clay mixtures containing various amount of Na MMT were mixed with BR and compounding ingredients according to the designed composition including zinc oxide 5 phr, stearic acid 2 phr, and dibenzothiazole disulfide 0.5 phr and heated at 60–70 °C; then, the diphenyl guanidine 0.5 phr, tetramethylthiuram disulfide 0.2 phr, sulfur 2 phr, and *N*-isopropyl-*N*-phenyl-*p*-phenylenediamine 1 phr were added together with the compound and mixed well followed by vulcanization process carried out at 150 °C for optimum cure time ( $t_{90}$ ), which is determined by an oscillating disk rheometer. The standard mold (2 mm × 110 mm) at 20 ton pressure was used for the compounding process of NR/BR/clay nanocomposites [26].

### 2.3.3 *Freeze-Drying*

Freeze-drying is the processing technique used to prepare NRNs at lower temperature. Generally, the natural rubber latex was mixed with the common vulcanization

ingredients with continuous stirring by using a homogenizer for 30 min at 70 °C; after this, the obtained mixture was mixed with 1 wt% nanofiller solution and stirred well for 2 h followed by 30 min homogenizing process. The coarse particles were filtered out to obtain the mixture solution of natural rubber latex, vulcanization ingredients, and nanofillers. The viscosity of this mixture solution was constantly monitored using suitable viscometer. Further, the obtained mixture was immediately frozen inside a cylindrical glass shell using liquid nitrogen flow. The frozen shells were loaded into a lyophilizer maintained at −54 °C with vacuum of less than 400 mtorr. The liquid phase of the compound in the ice form was sublimed to dry the compound followed by heating at 100 °C for 30 min to complete the vulcanization process and obtain the NRNs.

In a recent study, Rathanaawan Magaraphan et al. demonstrated the synthesis of natural rubber latex/clay aerogel nanocomposites using freeze-drying process. In a typical synthesis process, they have mixed the natural rubber latex with vulcanization ingredients. They have used a formulation consists of 60 % natural rubber, 10 % potassium hydroxide solution 0.5 phr, 50 % zinc oxide dispersion 1 phr, 50 % calcium carbonate dispersion 10 phr, 50 % sulfur dispersion 1 phr, 50 % zinc diethyl dithiocarbamate 0.75 phr, 50 % Wingstay-L dispersion 1 phr, and 1 % clay dispersion varying from 1 to 3 phr. All the ingredients listed above were thoroughly mixed together by continuous stirring by homogenizer at 70 °C for 30 min. The obtained solution was kept in tight plastic bottle. To prepare the nanocomposites with various concentrations of clay nanofillers, different weight percentage solutions of pristine clay fillers were added into the prevulcanized NR latex solution with vigorous stirring for 2 h, followed by stirring for 30 min at room temperature using homogenizer. After mixing, the prevulcanized NR latex solution was filtered to remove the coarse particles to obtain the nanocompounds. The obtained nanocompounds were kept in a cylindrical glass shell and subjected to liquid nitrogen flow for freezing the compound quickly. The frozen compound was attached to a lyophilizer maintained at −54 °C in a vacuum less than 400 mtorr for 36 h to sublime the ice in the compound. After subliming the ice completely out from the compound, the freeze-dried nanocompound was vulcanized at 100 °C for 30 min to obtain the natural rubber/clay nanocomposite [27].

### **2.3.4 *In Situ Non-aqueous Sol–Gel Method***

Due to the emerging trends in synthesis of rubber nanocomposites, unconventional methods like in situ non-aqueous sol-gel methods are inviting research interest due to its flexibility to make rubber nanocomposites incorporated with alkoxide-based fillers. Generally, in the in situ sol-gel method the natural rubber is made into the sheet form using conventional two-roll milling process, and the required amount of natural rubber was swollen for 24 h in required amount of organic solvent and the alkoxide precursor material was added into this swollen NR immersed in the solvent and mixed well in order to facilitate the homogenous mixing of alkoxide

precursor with the swollen rubber. Sequentially, the required amount of alcohol was added to the solution and after 30 min an appropriate amount of dilute acid solution was introduced into the above solution and stirred vigorously for a particular time. The reaction of alcohol with acid produces water, and this process will initiate the hydrolysis and condensation of alkoxide precursor. Thus, the in situ generation of alkoxides was propagated throughout the NR polymer matrix which leads to the in situ formation of nanostructured alkoxide fillers in the NR matrix. The final suspension was cast in a petri dish to remove the volatile content using aspiration hood. The obtained product was heated at 70 °C in a vacuum to prepare the NRNs followed by two-roll milling process to prepare them in sheet form. The in situ generated nanofillers are very much attractive due to their better surface interfacing properties which lead to the overall enhancement in mechanochemical properties of the NRNs.

Laura Wahba et al. recently reported the preparation of in situ sol-gel synthesis of NRNs loaded with silica nanofillers. They have reported the in situ non-aqueous sol-gel procedure in which the natural rubber sheets were swollen in required amount of toluene followed by the addition of TEOS precursor with vigorous stirring. As a result of thorough mixing, the silica precursor was intercalated into the NR polymer matrix, after the mixing process, required amount of ethanol is added into the toluene solution in which the NR was immersed and stirred for 30 min at 80 °C. Further, the required amount of carboxylic acid was added into the reaction mixture to initiate the in situ generation of water molecules, which activates the hydrolysis and condensation of TEOS precursor loaded in the NR matrix leads to the in situ formation of silica nanofillers. Then, the suspension was casted in a petri dish and kept inside an aspiration hood overnight to remove the volatiles. In conclusion, the obtained product was heated at 70 °C for 1 h under vacuum to remove the by-products to obtain the final NR nanocomposite product. The final nanocomposite product was reprocessed into the form of sheets using a conventional two-roll mill [28].

## **2.4 Characterization of Nanofillers and Natural Rubber Nanoblends**

Synthesis, fabrication, and characterization of natural rubber nanoblends are highly interdisciplinary research area. In this section, we would like to discuss the basic and advanced characterization techniques to understand the material properties for the benefit of the readers from different perspectives of science and technology. The physicochemical characterization of nanofillers can be done using various analytical techniques including X-ray diffractometry, UV–Visible spectrometry, photoluminescence spectrometry, vibrating sample magnetometry, Raman spectroscopy, scanning electron microscopy, energy-dispersive X-ray spectroscopy, transmission electron microscopy, selective area electron diffraction, thermo gravimetric and differential thermal analysis (DTA), differential scanning calorimetry, nanoindentation,

X-ray photon emission spectroscopy, electron probe microanalysis, X-ray fluorescence spectrometry, atomic force microscopy, and Fourier-transformed infrared spectroscopy.

### 2.4.1 X-ray Diffractometry (XRD)

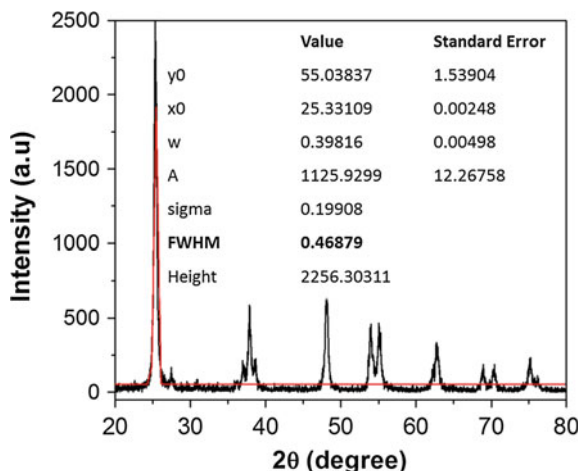
The X-ray diffraction technique is the most widely used characterization technique to investigate the crystal structure of the materials. In an ideal crystalline material, all the constituents are perfectly arranged in lattice and the lattice can extend in three-dimensional space. But in reality, the arrangement of constituents in a crystal are not perfectly ordered due to the lattice imperfections and stress which arises as a result of impurities, intrinsic, extrinsic defects, and lattice mismatch. Thus, the physicochemical properties of the materials are greatly affected by the crystal structure of the materials. The lattice planes in a crystal lattice of solid are of the order of 1 Å, and due to this, the X-ray wavelengths are compatible to interact with these lattice planes in the crystal. In XRD technique, the monochromatic X-ray beams generated from a controlled X-ray source is used to make a constructive interference pattern. According to Bragg's law,  $n\lambda = 2d \sin \theta$  where  $\lambda$  is the wavelength of the X-ray radiation,  $d$  is the interplanar distance between two successive atomic planes,  $\theta$  is the Bragg's angle (angle in which X-ray falls on the sample), and  $n$  is an integer number denotes the order of diffraction. The Miller indices ( $h, k, l$ ) of a hexagonal crystal structure can be related to Bragg's law using the following equation

$$1/d = 4/3 [(h^2 + hk + k^2)/a^2] + (l^2/c^2)$$

where  $a$  and  $c$  are the lattice constants.

The X-ray diffraction setup generally consists of four basic components: X-ray tube, Goniometer, sample holder and an X-ray detector. Generally, the Cu metal is used as the anode material for producing X-ray. The filament in the X-ray tube is heated to produce electrons and these electrons are accelerated by high voltage around 30–60 kV and guided to hit on target material fixed as anode. During the collision, the electron in the innermost K shell of the Cu metal will leave their space which will be occupied by the electrons in the outer shells such as L or M. Thus, the energy differences of the electrons are emitted as X-ray radiation generally named as  $K\alpha$  (energy difference of electrons from L shell) and  $K\beta$  (energy difference of electrons from M shell). We will deploy a filter to select  $K\alpha$  or  $K\beta$  radiation as per our convenience and requirement. Generally, Cu  $K\alpha$  (1.5405 Å) is used as a source due to the experimental convenience. The generated X-ray pattern can be compared with the standard diffraction pattern provided by the Joint Committee for Powder Diffraction Standards (JCPDS) or International Center for Diffraction Data (ICDD). Each crystalline material has its characteristic X-ray diffraction pattern, and by comparing the obtained pattern with the standard pattern, we can identify the crystal

**Fig. 2.3** X-ray diffractogram of TiO<sub>2</sub> nanoparticles



structure and phase of the crystalline material. In this way, XRD can be considered as the finger print technique to identify the material, structure, and phase. Considering the nanotechnological aspects, the crystallite size of the nanocrystalline material can be computed from the XRD patterns.

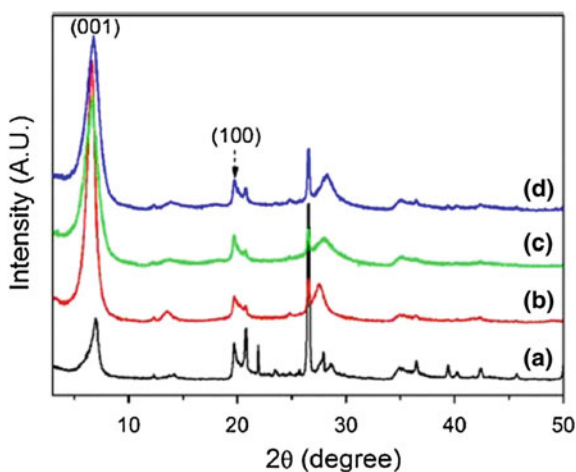
We can use different software packages to analyze the X-ray diffractogram. Generally, Origin software can be used to plot the XRD pattern and by selecting the signal processing option in the tool bar we can fit a Gaussian curve on the obtained XRD pattern which will give the full width half maximum (FWHM) for the dominant peak as shown in Fig. 2.3. Similarly, we can use various fittings for multiple peaks also to obtain their corresponding FWHM values. From the FWHM of the peaks in XRD pattern, the crystallite size of the nanomaterials can be calculated using Scherrer formula  $D = K\lambda / \beta \cos \theta B$  where  $D$  is the average crystallite size,  $\beta$  is the FWHM in radians of  $2\theta$ ,  $\lambda$  is the wavelength of the X-ray used,  $\theta B$  is the Bragg angle of the peak, and  $K$  is a constant equal to  $2(\ln 2/\pi)^{1/2} \approx 9$ . The NRNs can be characterized using XRD to understand the crystalline nature of the composite materials. The crystalline structure of nanofillers used to reinforce the natural rubber matrix can be identified from the XRD pattern, and we can get an idea about the influence of material processing and polymerization in growth and agglomeration of the nanofillers.

Generally, inorganic nanofillers used as the reinforcing agent have particular crystal structure and crystallite plane orientation which favors the catalytic nature of the fillers and these properties have direct influence on the physicochemical characteristics of the NRNs. The changes occurred in the crystal structure of the nanofillers are due to the exposure to heat, mechanical stress and strain. The crystal structure and average crystallite size of the nanofillers can be identified using XRD analysis. X-ray diffraction analysis helps us to confirm the incorporation of filler nanoparticles in the natural rubber matrix. In particular, the nanodimensional aspects of the fillers can be speculated from the geometrical behavior of the

obtained XRD pattern. The more broad the peaks in the XRD pattern, we can consider that the dimension of the fillers is projecting more toward the nanoregime and vice versa. The common mistakes take place during the XRD analysis of NRNs can be divided into two different categories. One is due to the fast scanning rate of XRD with a fixed sample stage. Since the amount of filler added into the natural rubber matrix is very small compared to the total volume of the composite, we have to provide enough exposure time of X-ray beams for effective diffraction in atomic planes that acquire more data points. In this case, fast scan is not preferred for analyzing NRN samples. To achieve XRD profiles with large data sets, a very small step size in the slow scan mode is advisable for the NRNs. If you take an XRD in fast scan mode, sometimes you will not be able to detect the corresponding diffraction peaks for the nanofillers or nanostructured reinforcing agents.

XRD technique can be used for understanding the structural changes happening to the filler during the interaction with NR, composite additives such as acids and activators. Figure 2.4a depicts the XRD patterns of MMT and Fig. 2.4b–d corresponds to the acid-treated MMT. The interaction of MMT with HCl leads to an increase in the crystallinity of the MMT filler, and this can be identified from the intensity of (001) plane. If the aim of the XRD analysis is to identify the effect of blending and processing techniques in the size and crystalline nature of the nanofillers, a systematic stepwise approach is required. Initially, we have to record the slow scan XRD pattern of natural rubber matrix and fillers separately, after that the XRD of the composite is recorded. We can utilize various types of computational packages such as X'Pert Pro, X'Pert High Score Plus, and Jana to compare graphical parameters obtained through the computational analysis of XRD spectra and derive the results through processing of simple algorithms consists of differential equations and polynomial functions. We can adopt different types of refinement methods to obtain a clear picture regarding the crystalline nature of the NRNs and their constituent components.

**Fig. 2.4** X-ray diffraction patterns of **a** pristine MMT, **b** 0.02 M HCl-treated MMT, **c** 0.1 M HCl-treated MMT, and **d** 0.5 M HCl-treated MMT “Adapted with permission from (doi:10.1021/am504426j | ACS Appl. Mater. Interfaces 2014, 6, 18769–18779). Copyright (2014) American Chemical Society”



### 2.4.2 X-ray Photoelectron Spectroscopy (XPS)

XPS analysis technique is used for the detection of dopants and impurities incorporated in the NRNs. Due to the advancements in nanotechnology, the development of NRNs for surface sensitive flexible membranes is fascinating enormous research interest among scientific communities across the globe. To analyze the physico-chemical properties of surface interface engineered NRNs, XPS can be used as a strong analytical tool. XPS is a versatile, nondestructive, chemical surface sensitive technique due to the limited ability of the low-energy X-ray radiation used in XPS to probe the uppermost atomic layers of the sample's surface. Generally, the probing depth of X-rays used in XPS is limited to 10 nm and the concentration of the elements of interest should exist in a minimum order of 0.1 atomic % or higher (Fig. 2.5).

As a result of inelastic scattering, the photoelectrons ejected during the XPS scan can travel only a very short distance to escape from the material and arrive at the detector without losing their kinetic energy. Due to this, we can get information regarding the materials present only in the few upper layers of atoms on the surface of the sample. In the XPS measurements, we measure the characteristic binding energies of the ejected core electrons using the Einstein's equation for photoelectric effect  $E_k = h\nu - E_b - W$ , where  $E_k$  and  $E_b$  are the kinetic and binding energy of the ejected electrons, respectively,  $h\nu$  is the energy of the incident X-ray photon and  $W$  is the combined work function of the sample and the spectrometer (Fig. 2.6).

The photoejected electrons are collected using electrostatic or electromagnetic lenses and then sent to an energy analyzer where the electrons are separated according to their corresponding kinetic energies. The received electrons are detected using a multichannel detector. The binding energy of the core-level electrons expressed in x-axis belong to the different atomic orbits while in the y-axis

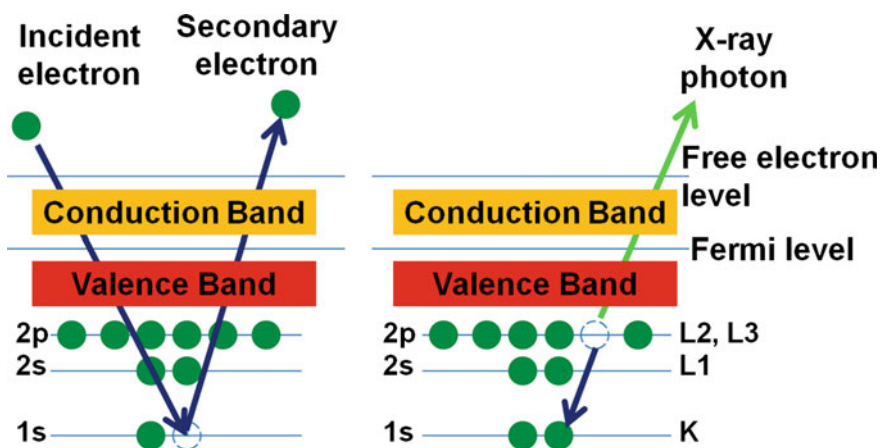
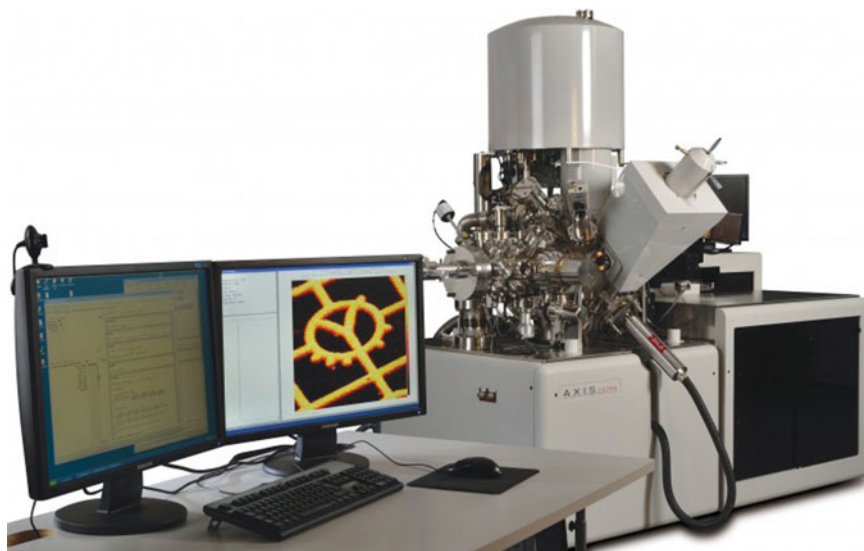


Fig. 2.5 Schematic of X-ray photoelectron emission process



**Fig. 2.6** X-ray photoelectron spectrometer

a series of photoelectron peaks where their relative intensities indicate the number of the outgoing electrons at each particular binding energy. The spectroscopic notation for the XPS spectral lines conventionally takes the form  $nl_j$ , which is different from the  $(2S+1)L_J$  atomic notation which describe the electron energy states in an atom. The letters  $n, l, j$  are the principal, the orbital angular momentum and the total angular momentum quantum numbers, respectively. Generally, the orbital angular momentum number is designated by the letter in lower case. The XPS is utilized to obtain both qualitative and quantitative information. Generally, a survey scan is recorded over a broad range of energies using wide steps (usually between 50 and 100 eV). Using this fast scan, we can identify the presence of elements and the amount of elements present which are enough for the detection range. The elemental surface concentration can be consistently assessed by integrating peak areas after excluding the background contribution caused by inelastic scattering.

Since the innermost electrons are shielded by the electrons in the outer shell, XPS measurement can be used to explore the oxidation state of the atom and the local chemical environment around the atom. The binding energies of core electrons are greatly affected by the chemical structure giving a small shift in the peak positions. This small shift is called a chemical shift, and it is related to the chemical state of the material. During the fast scan, we will be able to identify the binding energy range for typical chemical state of the particular atom. To identify the chemical shift, we have to perform a high-resolution scan over a selected narrow energy range, around one of the core-level peak, at small step sizes, typically (10–20) eV. The detailed line shape and small shifts in peak position can be easily

determined in the high-resolution XPS spectra. The ability to identify different oxidation states and chemical environments is considered as one of the major strength features of the XPS technique. The measured peak positions are compared to those documented standard database in order to calculate the chemical shift. Since the photoejected electrons are scattered by the gas molecules present in the analytical chamber of XPS instrument high vacuum is required to perform XPS experiments. High vacuum will enhance the mean free path of XPS electrons and make it possible to accurately measure the kinetic energy of the electrons. The charge cloud formation on the surface is a general problem in XPS measurements which causes the electrostatic “charging effect.” Because of the charging phenomena, XPS peaks would appear at higher binding energy than they should be. In order to overcome this static charging issue, charge neutralizer system was used to produce low-energy electrons to correct for the built-up charges. XPS technique can be used to analyze thin film, metal/natural rubber membranes, NRNs, etc. The NRN sample should be sectioned using a sample sizer before the XPS analysis. From the XPS spectra, we can identify the oxidation state of inorganic and organic materials and fillers present in the NRNs, and it will help us to understand the chemical bonding between the constituents in NRNs. We can use XPS technique to understand the chemical texture of noble metals implanted on the surface of the flexible natural rubber membranes of nanosensors. The XPS analysis is suggested as a strong tool to understand the chemical interaction between filler/reinforcement agent/curing agent and the natural rubber matrix (Figs. 2.7 and 2.8).

For example, Fig. 2.9a elucidates the wide-scan C1s XPS spectrum of olive residual and Fig. 2.9b shows high-resolution spectrum of the olive residual. From the high-resolution XPS spectra, we can find the different binding states of carbon. We can find out the chemical and oxidation states of elements present in the sample

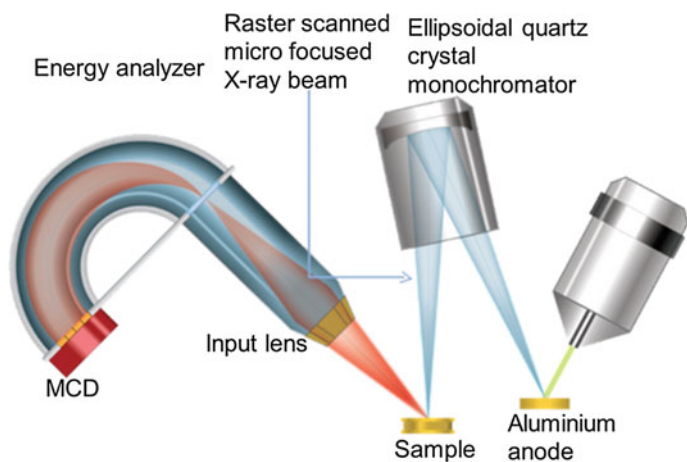


**Fig. 2.7** Schematic of energy analyzer system in XPS

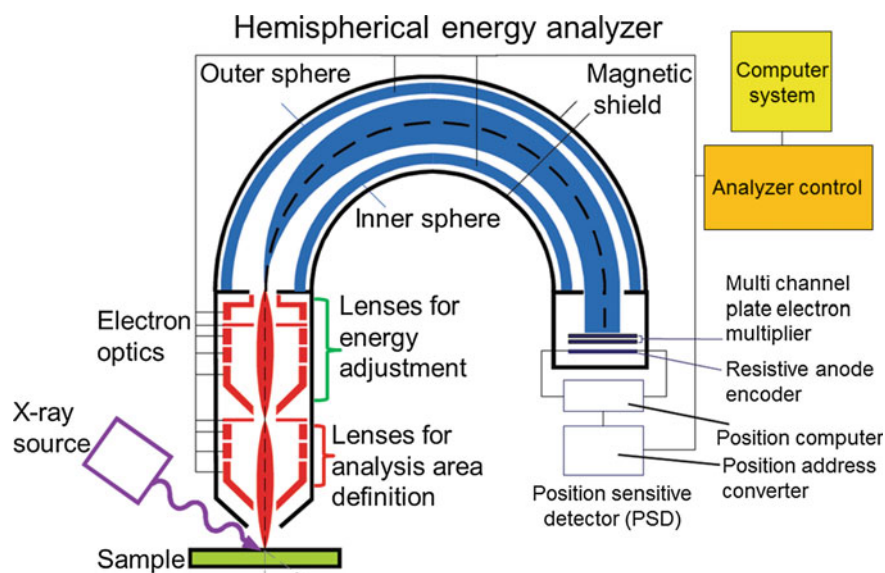


**Fig. 2.8** Block diagram of energy analyzer system in XPS

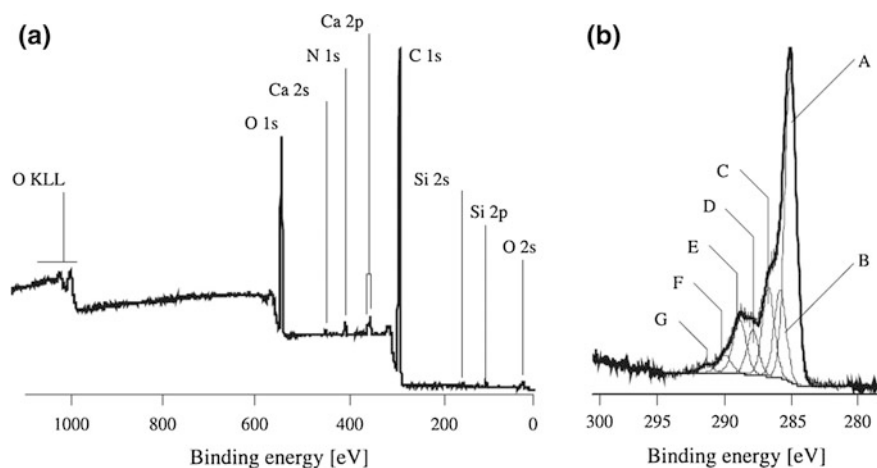


**Fig. 2.9** **a** Wide-scan and **b** high-resolution C1s XPS spectra of olive residual sample. “Adapted and licensed under a Creative Commons attribution-type from (Materials Research. 2012; 15(4): 671–678| doi:[10.1590/S1516-14392012005000086](https://doi.org/10.1590/S1516-14392012005000086)”

from their characteristic binding energy peaks. In a similar fashion, the physio-chemical characteristics of the nanofillers can be identified from the XPS analysis, and it also helps us to identify the surface polarity of the prepared nanocomposites.

### 2.4.3 *X-Ray Fluorescence Spectroscopy (XRF)*

X-ray fluorescence spectroscopy (XRF) is a nondestructive method used for elemental analysis of materials. An X-ray source is used to irradiate the specimen and to cause the elements in the specimen to emit (or fluoresce) their characteristic X-rays. A detector system is used to measure the positions of the fluorescent X-ray peaks for qualitative identification of the elements present and to measure the intensities of the peaks for quantitative determination of the composition. The technique is nondestructive, rapid, precise, and potentially very accurate. X-rays are electromagnetic radiation of very high energy (or short wavelength). When an X-ray photon strikes an atom and knocks out an innershell electron, if the incident photon has energy greater than the binding energy of the innershell electron, a readjustment occurs in the atom by filling the innershell vacancy with one of the outer electrons and simultaneously emitting an X-ray photon. The emitted photon (or fluorescent radiation) has the characteristic energy of the difference between the binding energies of the inner and the outer shells. The XRF wavelengths and relative intensities of a given element are constant to first approximation. Small changes may occur when the distribution of the outer (or valence) electron changes. A major area of research in XRF involves the use of “soft” X-ray emission (or long-wavelength XRF) spectra for chemical state analysis. Soft X-ray peaks often exhibit fine structure, which is a direct indication of the electronic structure (or chemical bonding) around the emitting atom. Thus, the shift in peak position, change in intensity distribution, or appearance of additional peaks can be correlated with a variety of chemical factors, including the oxidation state, coordination number, and nature of covalently bound ligands. The NRNs can be characterized using XRF technique to obtain the elemental and composition of the constituents in the rubber nanocomposite. The exact amount of additives and nanostructured fillers present in the composites can be identified quantitatively using this technique (Fig. 2.10).

### 2.4.4 *UV–Visible Spectroscopy*

The spectroscopic technique in which the ultraviolet and visible range of signals in the electromagnetic spectrum is utilized to study the samples is known as UV–Vis spectroscopy. We need a light source which gives the entire visible spectrum plus the near ultraviolet so that you are covering the range from about 200 nm to about 800 nm. (This extends slightly into the near infrared as well.) We cannot get this range of wavelengths from a single lamp, and so a combination of two is used—a deuterium lamp for the UV part of the spectrum, and a tungsten/halogen lamp for the visible part. When radiation interacts with matter, a number of processes can occur, including reflection, scattering, absorbance, fluorescence/phosphorescence (absorption and re-emission), and photochemical reaction (absorbance and bond

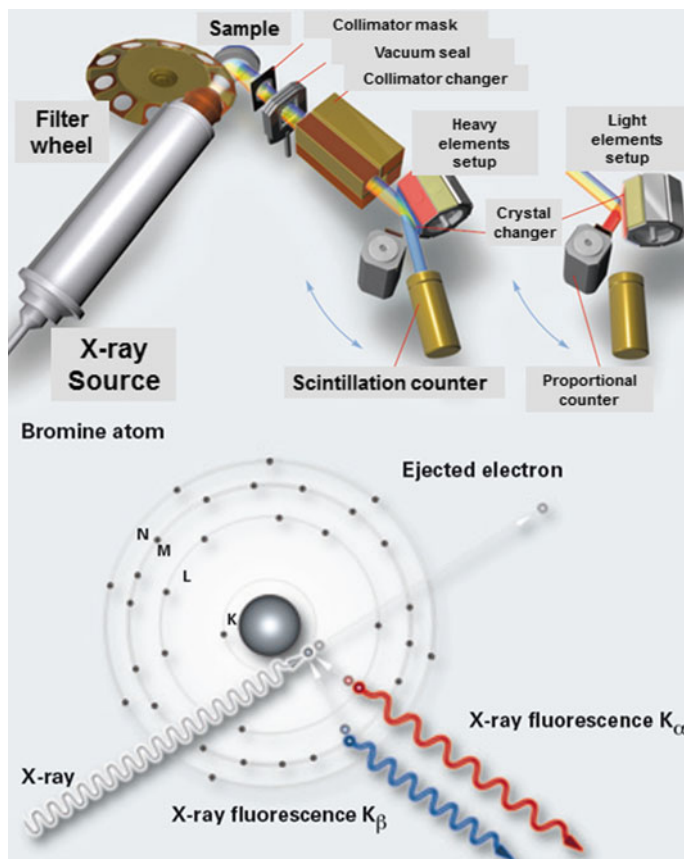


**Fig. 2.10** Schematic of X-ray fluorescence spectrometer

breaking). In general, when measuring UV–Vis spectra, we want only absorbance to occur. Because light is a form of energy, absorption of light by matter causes the energy content of the molecules (or atoms) to increase. The total potential energy of a molecule generally is represented as the sum of its electronic, vibrational, and rotational energies:  $E_{\text{total}} = E_{\text{electronic}} + E_{\text{vibrational}} + E_{\text{rotational}}$ . The amount of energy a molecule possesses in each form is not a continuum but a series of discrete levels or states. The differences in energy among the different states are in the order; in some molecules and atoms, photons of UV and visible light have enough energy to cause transitions between the different electronic energy levels. The wavelength of light absorbed is that having the energy required to move an electron from a lower energy level to a higher energy level.

When the input signal passing through the sample, the sample absorbs the energy from input UV–Vis signal and the electrons in the lower molecular orbitals jump into the excited higher molecular orbitals using the absorbed energy. So we

will get the output signal in which the wavelengths corresponding to the absorbed energy are absent. Thus, we will get particular peaks for the absorbed wavelength. By plotting a graph between absorptivity and wavelength, we can identify the chromophore from the corresponding peaks ( $\lambda_{\max}$ ) produced due to absorption of particular wavelengths. The band gap of the nanofillers can be found out using the equation given below:

$$\text{Band Gap Energy } (E) = h \times C$$

$h$  Planks constant =  $6.626 \times 10^{-34}$  J s

$C$  Speed of light =  $3.0 \times 10^8$  m/s

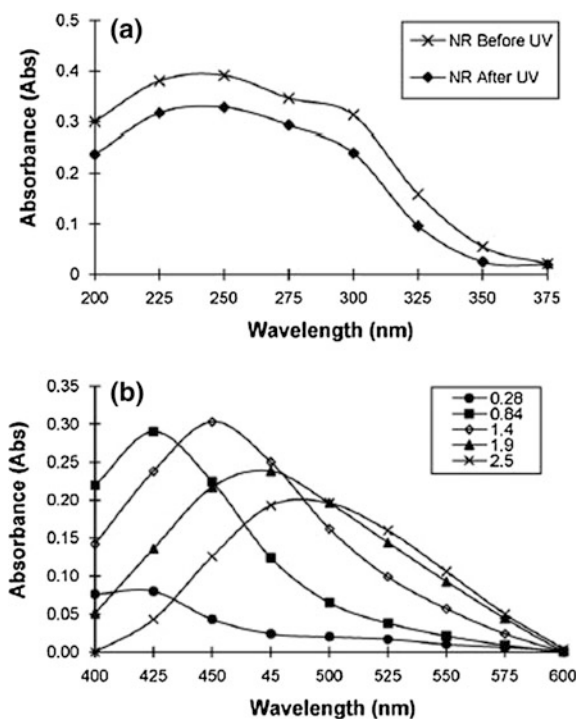
$\lambda$  Cutoff wavelength =  $\lambda_{\max} \times 10^{-9}$  m

$E$  Energy in electron volt (eV)

where  $1 \text{ eV} = 1.6 \times 10^{-19}$  J (conversion factor)

Recently, Baker NHHA et al. demonstrated the synthesis and characterization of silver nanoparticles in natural rubber. The presence of silver nanoparticle in the natural rubber was identified using UV–Vis spectroscopy as shown in Fig. 2.11. The broad characteristic absorption band of NR was obtained at  $\lambda_{\max} = 239$ . During the composite formation, the silver nanoparticle are incorporated into the NR matrix and this can be identified from the variation in absorption band with in the range of

**Fig. 2.11** UV–Vis absorption spectra: **a** natural rubber and **b** NR–silver composite at various concentrations,  $\times 10^{-3}$  M. “Adapted from N.H.H. Abu Bakar et al. Materials Chemistry and Physics 104 (2007) 276–283”



425–484 nm with varying silver nanofillers concentration. UV–Vis-based spectroscopic techniques can be easily adopted for identifying the presence of optically active nanofillers in the prepared NRNs.

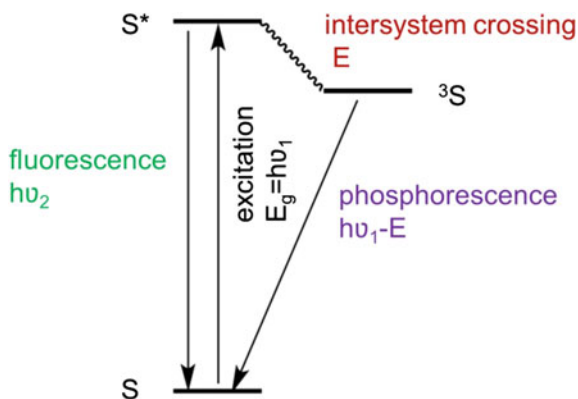
### 2.4.5 Photoluminescence Spectroscopy

Photoluminescence spectroscopy is considered as one of the most important method to identify the optical luminescence of the nanomaterials (Fig. 2.12).

Photoluminescence (PL) is the spontaneous emission of light from a material under optical excitation. PL measurement is a kind of powerful and nondestructive technique to identify the semiconducting and nanometal fillers in NRNs. Various ranges of wavelength are used to carry out the PL measurements. Generally, during PL measurements the NRNs was excited with a selective wavelength around the band gap ( $E_g$ ) of the composite, which were already determined by using UV–Vis spectroscopy methods.

When the light of sufficient energy is illuminated a composite consisting of semiconducting or metal nanofillers, photons are absorbed and excitations are created. These excited carriers will undergo relaxation by emitting a photon. These emission spectra can be analyzed to identify the optical and surface interfacing properties of the nanofillers. In PL measurements of NRN, only the photons with equal to or higher energy than the band gap of the nanocomposites/nanofiller were absorbed. Therefore, we have to choose different excitation source to do the measurements according to different filler/nanocomposites material with different electronic band structure. The PL peak positions reveal the energy transitions, and the PL intensity indicates the relative rates of radiative and non-radiative recombinations occurring during the excitation process. We can change other external parameters during the PL measurement, such as temperature, excitation power, and applied external perturbation such as magnetic field, electrical field, and pressure.

**Fig. 2.12** The fluorescence and phosphorescence energy transfer



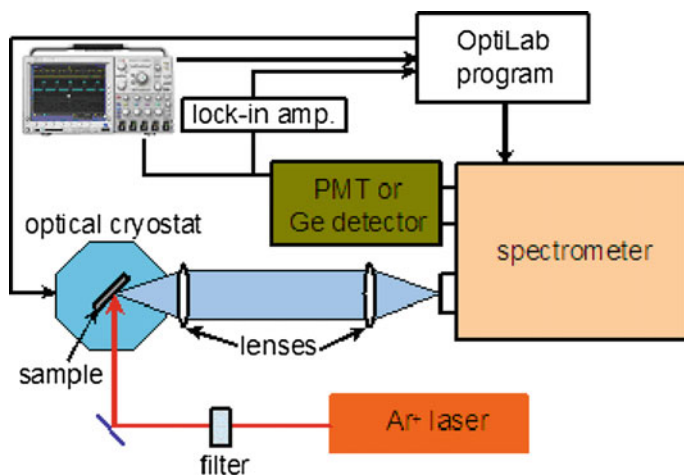


**Fig. 2.13** Block diagram of a photoluminescence spectrophotometer

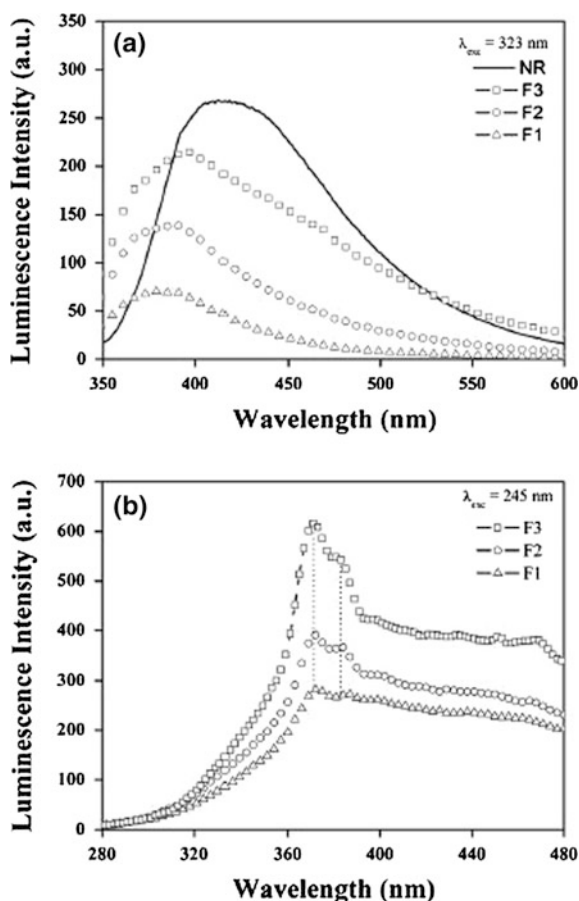
This will help us for understanding the electronic states and bands. Various information including band gap of nanofillers, impurity levels and defects, material quality, recombination mechanism, and surface plasmon resonance properties of nanofillers can be obtained from the PL spectra (Fig. 2.13).

Recently, Cabrera FC et al. demonstrated the Au/NR nanocomposite synthesis in which the authors were successfully synthesized the NR/Au nanocomposite. The research group collected the emission spectra of natural rubber excited at 380 nm and obtained various emission maxima as shown in Fig. 2.14. The bands are at 371 and 382 nm. The shift in this PL bands can provide various information including recombination kinetics and dynamics of natural rubber, nanofillers, and NRNs. The same method can be used for identifying and understanding the change in fluorescence of the NRN due to the incorporation of nanofillers such as metal nanoparticles and metal oxides.

#### 2.4.6 Raman Spectroscopy

Raman spectroscopy is widely used to analyze structural and chemical properties of the nanofillers. In Raman spectroscopy, the sample is illuminated by monochromatic light like laser light. During the illumination process, a very small proportion of the incident radiation interacts with the vibrational energy levels in the sample and exchanges energy as a result of this interactions. The scattered light that has undergone an energy change is called as Raman scattered light. Raman scattered light has energies lower or higher than those of the incident light, and this energy change is equal to the vibrational energies of the sample. This energy results a rise to the peaks in a Raman spectrum and the amount of the peak shift which is referred

**Fig. 2.14** Emission spectrum evaluated using excitation light at wavelengths **a** 323 nm and **b** 245 nm. Measured for both NR membranes and different latex phases thin films NR, natural rubber. “Adapted from Cabrera FC et al. Luminescence 2014; 29: 1047–1052”



as shift in energy from the incident light is called as the Raman shift. In a detailed aspect, we can consider Raman spectroscopy as one of the advanced characterization technique which measures the inelastic scattering of the light over the sample. Raman spectroscopy is used to measure the vibrational modes present in a molecule. A key difference between the Raman and infrared processes is that, in the former process, the photons involved are not absorbed or emitted but rather shifted in frequency by an amount corresponding to the energy of the particular vibrational transition. In the Stokes process, which is the parallel of absorption, the scattered photons are shifted to lower frequencies as the molecules abstract energy from the exciting photons; in the anti-Stokes process, which is parallel to emission, the scattered photons are shifted to higher frequencies as they pick up the energy released by the molecules in the course of transitions to the ground state. In addition, a substantial number of the scattered photons are not shifted in frequency. The process which gives rise to these photons is known as Rayleigh scattering.

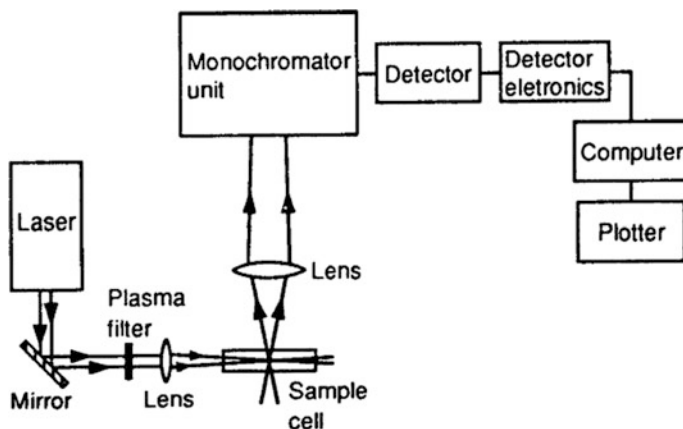
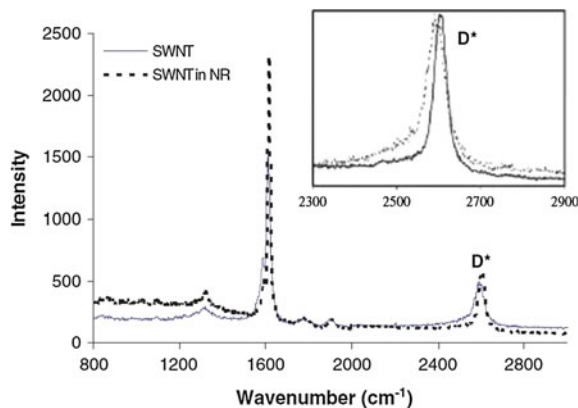


Fig. 2.15 Schematic diagram of a Raman spectrometer

To be active in the infrared spectra, transitions must have a change in the molecular dipole associated with them. For Raman activity, in contrast, the change has to be in the polarizability of the molecule. A typical Raman spectrometer consists of the following basic components: (1) an excitation source, usually a laser; (2) optics for sample illumination; (3) a double or triple monochromator; and (4) a signal processing system consisting of a detector, an amplifier, and an output device. A diagram showing various components of the Raman spectrometer is shown in Fig. 2.15. A number of stages are involved in the acquisition of Raman spectrum. A sample is mounted in the sample chamber and laser light is focused on it with the help of a lens.

Generally, liquids and solids are sampled in a Pyrex capillary tube. The scattered light is collected using another lens and is focused at the entrance slit of the monochromator. Monochromator slit widths are set for desired spectral resolution. The monochromator effectively rejects stray light and serves as a dispersing element for incoming radiation. The light leaving the exit slit of the monochromator is collected and focused on the surface of a detector. This optical signal is converted to an electrical signal within the detector and further manipulated using detector electronics. The Raman spectrum will give a clear picture about the chemical composition, crystallite characteristics such as orientation, lattice strain, and crystal orientations. The spectral parameters concomitant with the Raman spectra can be attributed to various physicochemical aspects of the sample in such a way that the characteristic Raman frequency gives an idea about the composition and identity of the material, polarization of Raman peak provides information about the crystal symmetry and orientation, changes in frequency of Raman peak correspond to the stress or strain in the crystal lattice of the analyzed sample, and width and intensity of the Raman peak deliver the information regarding quality and quantity of the constituent materials in the sample (Fig. 2.16).

**Fig. 2.16** Typical Raman spectra of SWNTs in air (dotted line) and SWNT/NR composite (solid line). The insert graph is the enlarged spectrum around the D\* peak. “Adapted from Zhao Q et al. Carbon 44 (2006) 1740–1745”



Recently, Zhao Q et al. used Raman spectroscopic techniques to understand the vulcanization process in single-wall nanotube and natural rubber. Surface interface properties of the nanocomposite determine the degree of polymer molecular slip-page over the SWNT. The composite formation of SWNT fillers in NR matrix can be identified from the D\* peak shift of the SWNTs to a higher frequency when it is embedded in the NR matrix.

#### 2.4.7 Thermogravimetric Analysis and Differential Thermal Analysis (TGA-DTA)

Thermal analysis is the analysis of a change in a property of a sample, which is related to an imposed change in the temperature. The sample is usually in the solid state, and the changes that occur on heating include melting, phase transition, sublimation, and decomposition can be analyzed using thermal analysis. The analysis of the change in the mass of a sample on heating is known as thermogravimetric analysis (TG). TG measures mass changes in a material as a function of temperature under a controlled atmosphere. Its principal uses include measurement of a material's thermal stability and composition. TG is most useful for dehydration, decomposition, desorption, and oxidation processes. The most widely used thermal method of analysis is DTA. In DTA, the temperature of a sample is compared with that of an inert reference material during a programmed change of temperature. The temperature should be the same until thermal event occurs, such as melting, decomposition, or change in the crystal structure. In an endothermic event takes place within the sample, the temperature of the sample will lag behind that of the reference and a minimum will be observed on the curve. On the contrary, if an exothermal event takes place, then the temperature of the sample will exceed that of the reference and a maximum will be observed on the curve (Fig. 2.17).

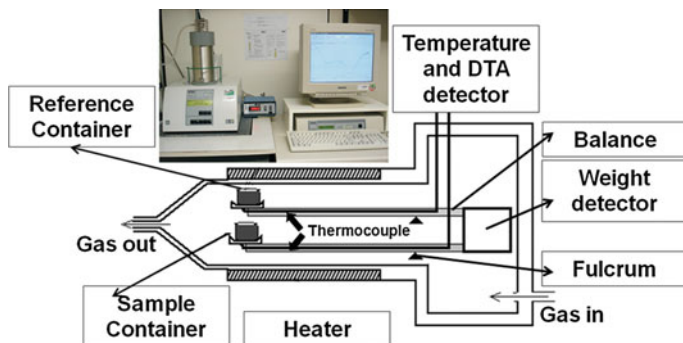


**Fig. 2.17** Schematic of TG/DTA

The TG/DTA apparatus consists of 2 cuvettes, one for the sample to be analyzed and the other is the reference. In TGA analysis, the weight loss of the sample is measured as a function of temperature. But, in the case of DTA analysis, the change in temperature of the sample and the reference is measured as a function of the temperature.

The most widely used thermal method of analysis is DTA. In DTA, the temperature of a sample is compared with that of an inert reference material during a programmed change of temperature. The temperature should be the same until thermal event occurs, such as melting, decomposition or change in the crystal structure. In an endothermic event takes place within the sample, the temperature of the sample will lag behind that of the reference and a minimum will be observed on the curve. On the contrary, if an exothermic event takes place, then the temperature of the sample will exceed that of the reference and a maximum will be observed on the curve.

The TG/DTA apparatus consists of 2 cuvettes, one for the sample to be analyzed and the other is the reference. In TGA analysis, the weight loss of the sample is measured as a function of temperature. But, in the case of DTA analysis, the change in temperature of the sample and the reference is measured as a function of the temperature. TG/DTA can be used to find out various material properties such as melting temperatures, transition enthalpies, phase transformations, phase diagrams, crystallization temperatures, degree of crystallinity, glass transition temperatures, decomposition effects, reaction kinetics, and purity determinations.

Carrado et al. determined the percentage of final polymer loading in polymer clay by DTG analysis. Figure 2.18 displays DTG curves for synthetic Li-hectorite and its polymer hectorite derivatives. DTG peak at 67 °C corresponds to the surface water loss, and at 730 °C dehydroxylation of the clay layers occurs. The percentage of weight loss over the temperature range varying from 200 to 600 °C provides the information regarding the polymer loading.

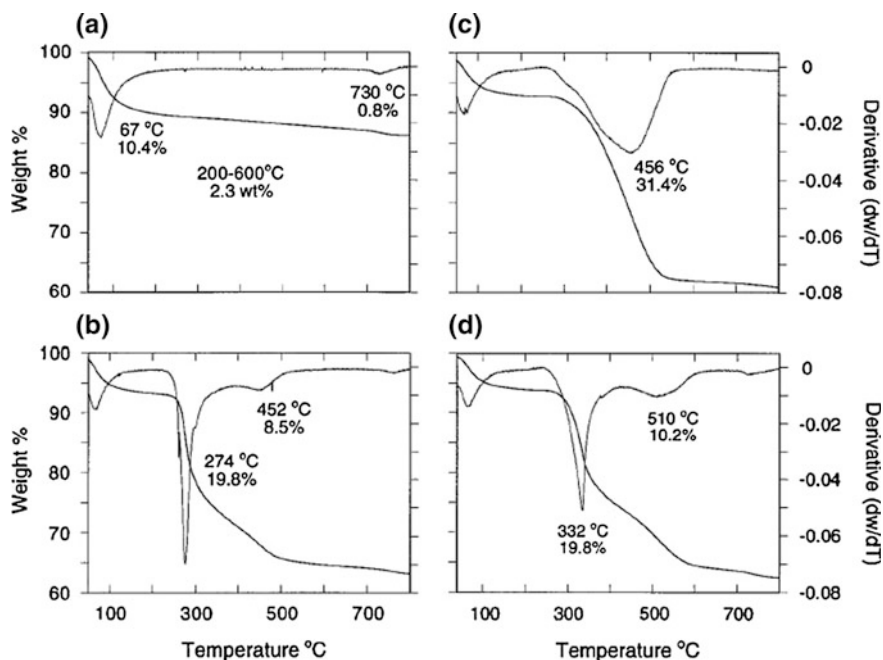


**Fig. 2.18** TGA and DTG curves for synthetic hectorite preparations: **a** Li, **b** HPMC-2 (20 %), **c** PANI-2 (20 %), and **d** PVP-3 (20 %). “Adapted from Carrado KA et al. Chem. Mater. 1998, 10, 1440–1445”

#### 2.4.8 Scanning Electron Microscopy-Energy-Dispersive X-Ray Spectroscopy (SEM-EDX)

The scanning electron microscope (SEM) is a type of electron microscope that helps in forming an image of the sample surface by scanning. The electrons in the beam interact with the atoms in the surface to generate signals that provides properties such as composition, topography, and electrical conductivity. The signals produced by an SEM include secondary and back-scattered electrons, characteristic X-rays, specimen current, and light due to cathodoluminescence. All SEMs usually have the ability to detect secondary electrons. SEM helps in obtaining high-resolution images of samples ranging in size from those visible to the naked eye to those which are just a few nanometers in size. In most of the applications, the data collected are over a preselected area of the sample surface, and following this, a 2D image is generated that shows the various spatial variations. Conventional SEMs with a magnification range of 20X–30000X with a spatial resolution of 50–100 nm can scan areas which vary from 1 cm to 5  $\mu\text{m}$  in width. SEMs also

have the ability to analyze particular points as can be seen during electron energy X-ray diffraction (EDX) operations which help in determining the chemical composition of the sample concerned. Energy-dispersive X-ray analysis, also known as EDS, EDX or EDAX, is a technique used to identify the elemental composition of a sample. During EDS, a sample is exposed to an electron beam inside a scanning electron microscope (SEM). These electrons collide with the electrons within the sample, causing some of them to be knocked out of their orbits. The vacated positions are filled by higher energy electrons which emit X-rays in the process. By analyzing the emitted X-rays, the elemental composition of the sample can be determined. EDS is a very handy tool for performing the constitutional analysis of any kind of material. Secondary electrons and backscattered electrons are most commonly used for the purpose of imaging samples: secondary electrons depict morphology and topography of the samples while backscattered electrons depict contrasts in composition in multiphase samples. X-rays are produced when incident electrons collide in elastically with the electrons of the atoms in the sample. As the excited electrons get back to their previous positions, they emit X-ray which is the characteristic property of a material. The schematic diagram of a SEM is shown in Fig. 2.19.

Essential components of all SEMs include the following:

- Electron source (“gun”),
- Electron lenses,
- Sample stage,
- Detectors for all signals of interest, and
- Display/data output devices.

Infrastructure requirements:

- Power supply,
- Vacuum system,
- Cooling system,
- Vibration-free floor, and
- Room free of ambient magnetic and electric fields (Fig. 2.20).

Figure 2.21 shows the cryogenic fracture surfaces of the NRN loaded with various concentrations of carbon black fillers.

#### **2.4.9 Electron Probe Microanalyzer (EPMA)**

The principle of an electron microprobe is that if a solid material is bombarded by an accelerated and focused electron beam of sufficient energy it can liberate both matter and energy from the sample. These electron–sample interactions mainly

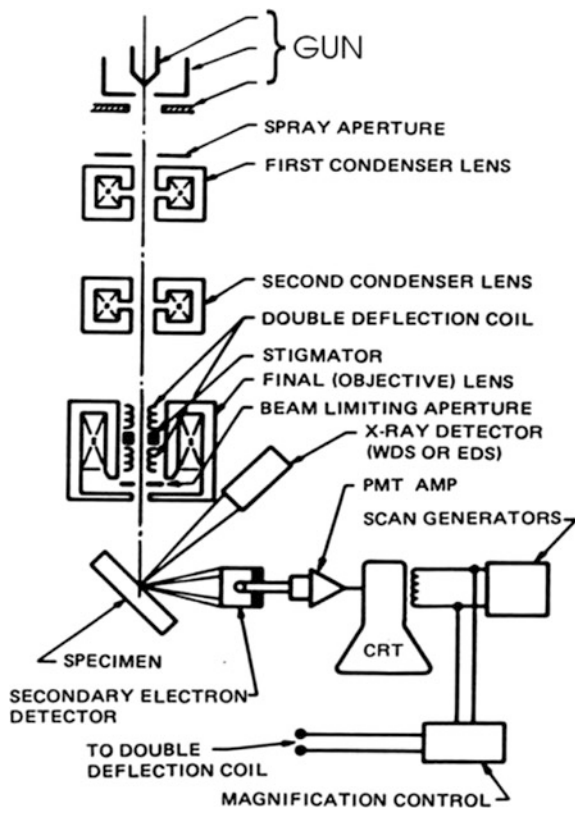


Fig. 2.19 Schematic diagram of a SEM

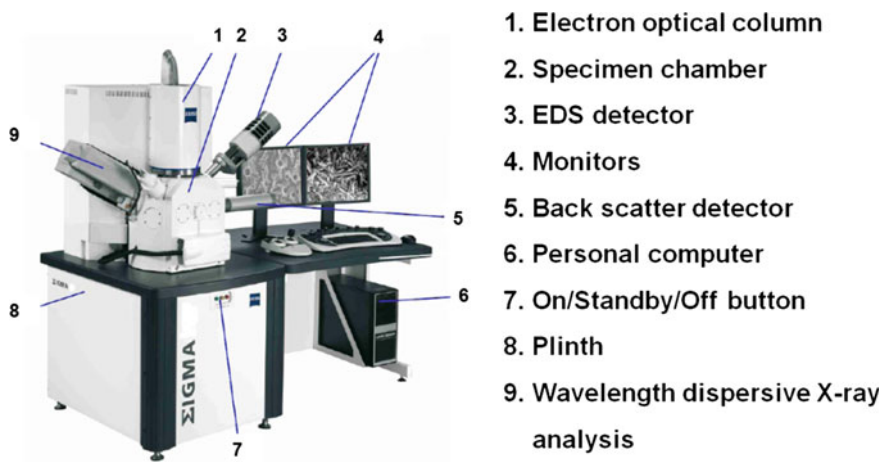
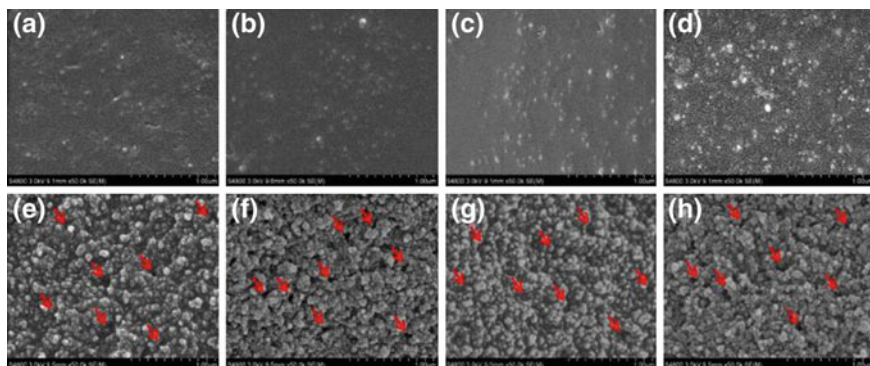


Fig. 2.20 Diagram showing the components of scanning electron microscope



**Fig. 2.21** SEM images of cryogenic fracture surfaces of the samples **a** NR40, **b** NR50, **c** NR60, **d** NR70; **e** CBG40, **f** CBG50, **g** CBG60, and **h** CBG70. *Arrows show the pores in CBGs.* “Adapted with permission from Gan S et al. *Macromolecules*, 2016, 49 (4), 1454–1463.” Copyright (2014) American Chemical Society

liberate heat, but electrons and X-rays are also generated. Of most common interest in the analysis of materials are secondary and back-scattered electrons, which are useful for imaging a surface or obtaining an average composition of the material. X-ray generation is produced by inelastic collisions of the incident electrons with electrons in the inner shells of atoms in the sample; when an innershell electron is ejected from its orbit, leaving a vacancy, a higher-shell electron falls into this vacancy releasing some energy in the form X-rays. These X-rays are characteristic of the element and are quantized to determine the elemental composition. EPMA analysis is considered to be “nondestructive”; that is, X-rays generated by electron interactions do not lead to volume loss of the sample, so it is possible to reanalyze the same materials more than one time.

In EPMA, the elemental composition of the constituent nanomaterials is measured by recording wavelength dispersive spectra of the samples. During the EPMA analysis, the microvolume of the samples was exposed to a focused electron beam and collecting the X-ray photons generated by various constituent elements present in the nanocomposites. The sample composition can be identified from the wavelength dispersive spectra (WDS) recorded. EPMA can be used to detect the presence of fillers and constituents in NRNs with ppm sensitivity. Generally, electron beams with energy varying from 5 to 30 keV are usually used to carry out the EPMA measurements. Compared to the SEM-EDX analysis, the EPMA analysis provide much better results due to the superior ability of WDS to detect the elements with high sensitivity. The detector dead time and spectral resolution of EPMA are better than that of energy-dispersive spectrometer. Also the thickness of

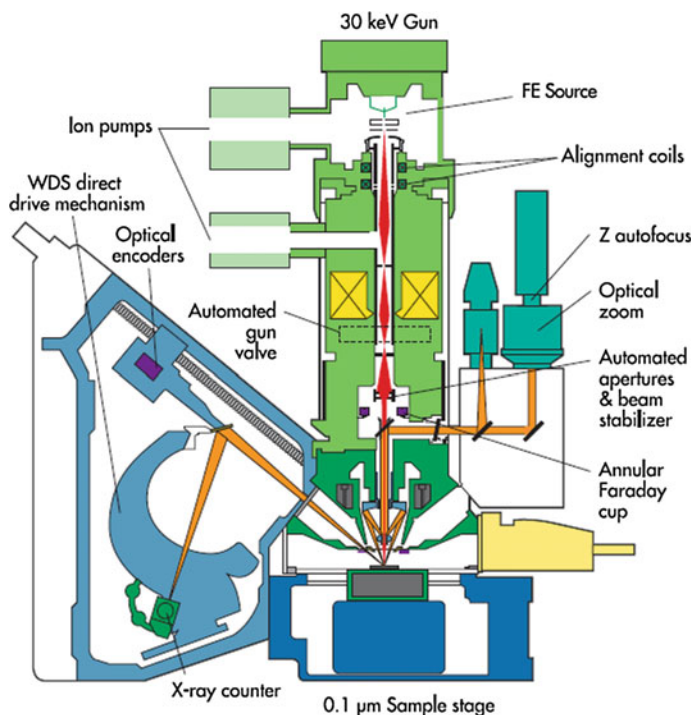


Fig. 2.22 Block diagram of electron probe microanalyzer

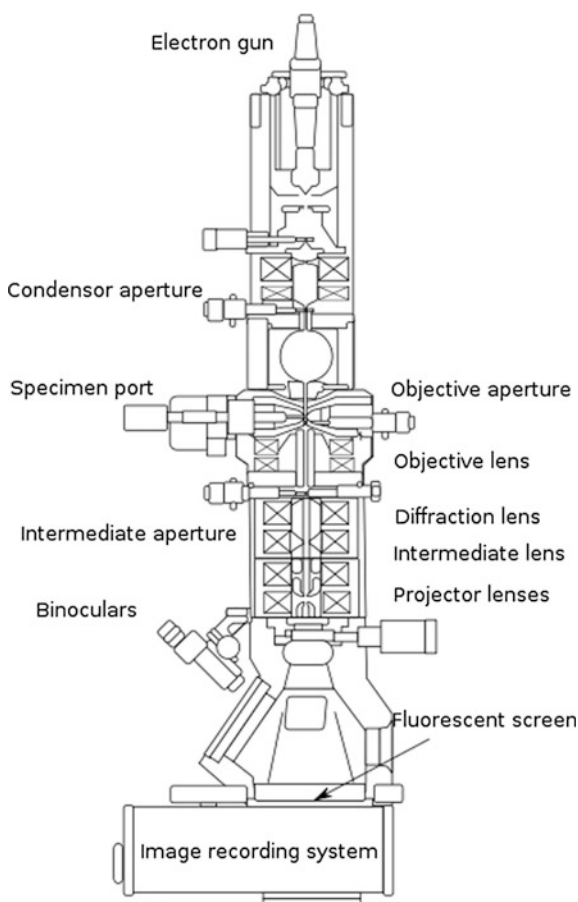
the nanofiller layers with size varying from nanometer to millimeter range can be measured using EPMA system with its flexible sample analysis abilities and magnification setup ranging from 40 to 400,000 (Fig. 2.22).

#### 2.4.10 *Transmission Electron Microscopy-Selected Area Electron Diffraction (TEM-SAED)*

Transmission electron microscopy is widely used to study the surface morphology and topology of the nanomaterials. In TEM analysis, a beam of electrons are allowed to undergo transmission through a thin specimen which can transmit the electrons. During the transmission, the electrons will interact with the specimen and the image formed due to the result of these interactions is magnified and focused on to a fluorescent screen. The advanced image detection technique like CCD cameras is also used for the digital image formation in TEM analysis. In comparison with the conventional light microscopes, since the electrons used in TEM analysis have small de Broglie wavelength, it can be used for very-high-resolution imaging purpose. Due to his high-resolution imaging ability, TEM analysis can reveal the

fine details of even single atom or columns of atoms. TEM forms a major analysis method in a range of scientific fields, in both physical and biological sciences. Recent development in NRNs has attracted researchers to utilize the TEM technique to characterize the nanofillers and polymers incorporated into the nanocomposites during the manufacturing process. TEM characterization of nanofillers and nanocomposites provide crucial information regarding the topology and morphology of the nanofillers and reinforcing agents incorporated in the NR matrix. It includes the nature of surface interaction and influence on compounding on forming extra cross-linking sites over the nanofillers. The high-resolution TEM images of nanofillers forms a clear picture regarding the real time distribution of those filler materials inside the NR matrix. TEM analysis will help the researchers to extract information regarding mechanochemical properties of the NRNs by understanding the morphology and cross-linking dynamics of the nanofillers from the TEM pictures. Grain boundary interactions of the multiphase blends with nanofillers can be elucidated from the TEM analysis (Fig. 2.23).

**Fig. 2.23** Block diagram of basic TEM



Selected area electron diffraction is a crystallographic characterization method which is utilized hand to hand with TEM analysis. In the SAED analysis, the electrons are targeted on a typical spot in the specimen and allowed to transmit through it, and an aperture in the image plane is used to select the diffracted region of the specimen, giving site-selective diffraction analysis. The atoms in the electron transparent specimen will act as a diffraction grating to the electrons, and due to this, the transmitted electrons are diffracted and scattered to different directions and particular angles. This will form images of series of spots or rings on the screen of the TEM. We can generate the required condition for a specific kind of diffraction by tilting and rotating the samples. The diffraction pattern obtained by this kind can provide the information including crystallinity of the sample, crystal structure of the sample and orientation of the crystal planes of the samples, etc. The crystalline samples can be tilted to a low-index zone axes to identify the crystal structures and measure lattice parameters. SAED of nanocrystals gives ring patterns analogous to those from X-ray powder diffraction and can be used to identify texture and discriminate nanocrystalline from amorphous phases (Fig. 2.24).

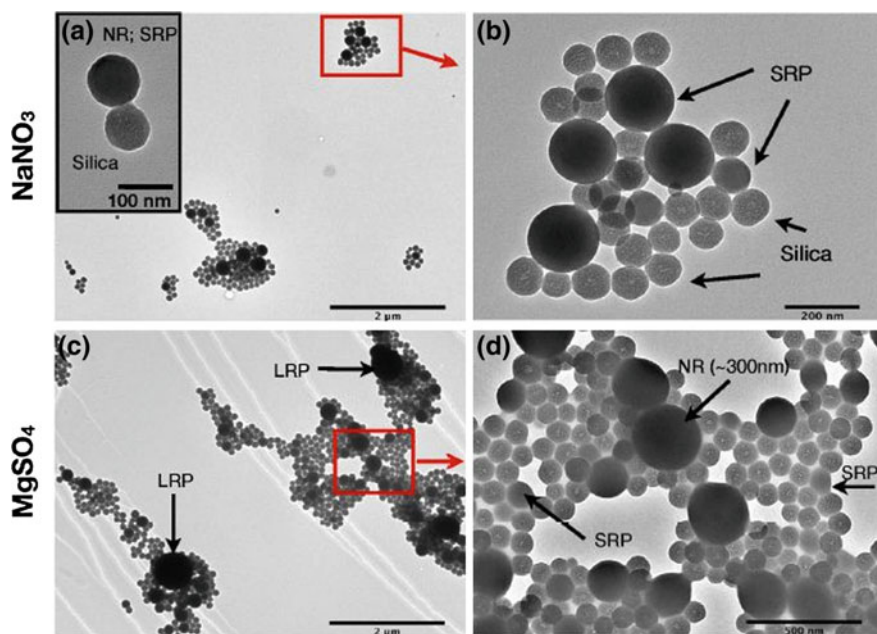


**Fig. 2.24** TEM micrographs of NR-100 nm plain silica after 2 h of interaction in (a, b)  $\text{NaNO}_3$  and (c, d)  $\text{MgSO}_4$  suspensions at 100 mM ionic strength. **b** and **d** Magnified image of the red rectangular zone in (a) and (c), respectively. *Inset* in (a) magnified image of a 1:1 NR-plain silica particle interaction. “Adapted with permission from Chan AJ et al. *Langmuir*, 2015, 31 (45), 12437–12446.” Copyright (2014) American Chemical Society

### 2.4.11 Vibrating Sample Magnetometry (VSM)

Vibrating sample magnetometry (VSM) is based on the Faraday's law which states that an electromagnetic force is generated in a coil when there is a change in flux linking the coil. In the measurement setup, a magnetic sample is moving in the vicinity of two pickup coils as given in Fig. 2.25. The oscillator provides a sinusoidal signal that is deciphered by the transducer assembly into a vertical vibration. The sample which is fixed to the sample rod vibrates with a given frequency and amplitude (60 Hz and  $\sim 1$  mm, respectively). The sample is centered between the two pole pieces of an electromagnet that generates a magnetic field ( $H_0$ ) of high homogeneity. Stationary pickup coils are mounted on the poles of the electromagnet. Their symmetry center coincides with the magnetic center of the sample. Hence, the change in magnetic flux originating from the vertical movement of the magnetized sample induces a voltage  $V_{\text{ind}}$  in the coils. This induced voltage is a measure of the magnetic moment of the sample. The VSM characterization technique is widely used to investigate the magnetic properties of the NRNs containing magnetically active filler nanoparticles such as  $\text{Fe}_2\text{O}_3$ ,  $\text{ZnO}$ , and  $\text{Gd}_2\text{O}_3$  (Fig. 2.26).

**Fig. 2.25** Schematic representation of a VSM

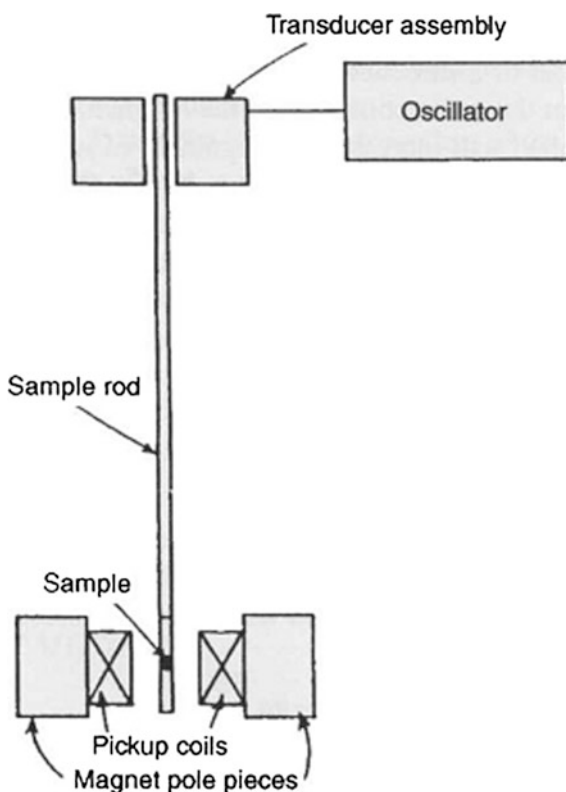
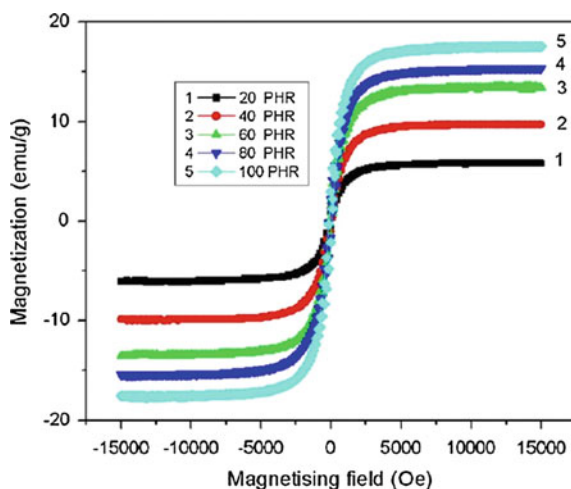


**Fig. 2.26** Magnetic hysteresis of composites measured on VSM. The rubber composites show a ferromagnetic behavior and the saturation magnetization is found to increase with the nickel filler content. “Adapted from Jamal EMA et al. Materials Science and Engineering B 156 (2009) 24–31”



#### 2.4.12 Fourier Transform Infrared Spectroscopy (FTIR)

Fourier transform infrared (FTIR) spectroscopy is one of the most common spectroscopic techniques used by organic and inorganic chemists. It is the absorption measurement of different IR frequencies by a sample positioned in the path of an IR beam. The crucial goal of IR spectroscopic analysis is to determine the chemical functional groups in the sample. Different functional groups absorb characteristic frequencies of IR radiation. IR spectroscopy is an important tool for identification and elucidation of NRNs. At temperatures above absolute zero, all the atoms in molecules are in continuous vibration with respect to each other. When the frequency of a specific vibration is equal to the frequency of the IR radiation focused on the molecule, the molecule absorbs the radiation. The resulting spectrum represents the molecular absorption and transmission, creating a molecular fingerprint of the sample. Like a fingerprint, no two unique molecular structures produce the same infrared spectrum. This makes infrared spectroscopy useful for numerous types of analysis (Fig. 2.27).

The FTIR technique is used to identify the functional groups present in the polymer blends and nanofillers in NRNs. The adsorption and surface interaction of natural rubber with various nanopolymers and nanofillers can be easily identified from the FTIR spectra by assigning the vibrational modes to the obtained FTIR spectra and comparing it with the FTIR modes of standard functional groups (Fig. 2.28).

**Fig. 2.27** Block diagram of an FTIR spectrometer

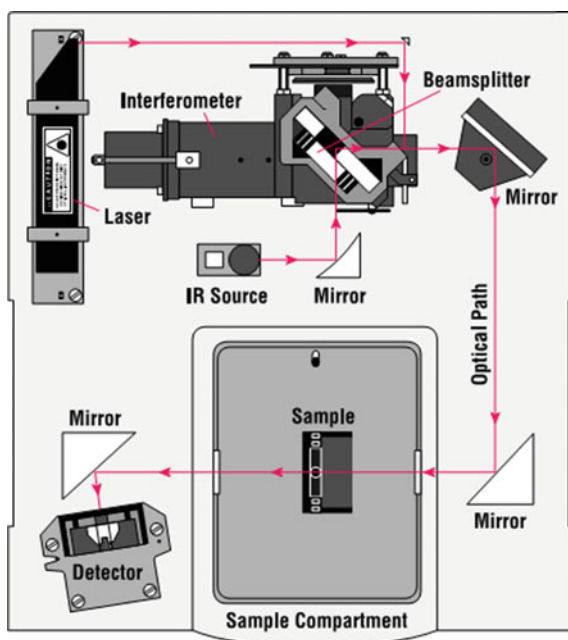
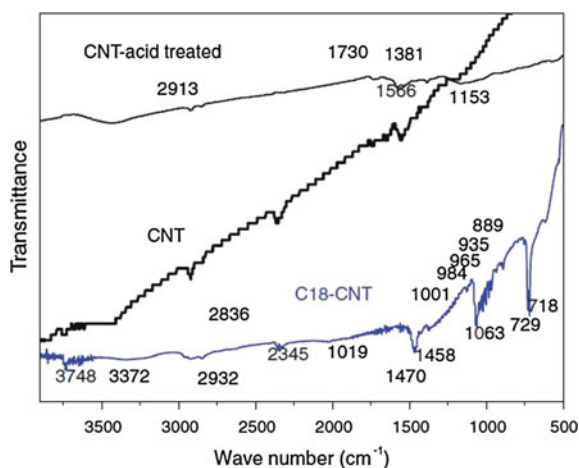


**Fig. 2.28** FT-IR spectra of CNT, CNT treated with acid and C18-CNT. “Adapted from Thomas PS et al. J Mater Sci (2012) 47:3344–3349”



## 2.5 Novel Nanofillers for Developing NRNs and Their Applications

Fillers are generally defined as the class of materials or additives which are added into the NR matrix to reinforce and enhance the physicochemical and mechanical properties of the NR in a desired manner. To achieve the required material

properties for industrial and technological applications, we have to add large amount of fillers into the NR matrix, which affects the transparency and brittleness and chemical properties of the natural rubber-based materials. Due to this type of issues associated with conventional fillers in the size range of micrometers, there is a research interest among scientist communities across the globe to develop new materials for filler applications. Recent trends in nanotechnology facilitated the development of nanomaterials for filler applications provided a tremendous upthrust in natural rubber industry. Nanomaterial-based fillers have unique properties including high surface to volume ratio, tunable surface energy and physicochemical properties which provide large surface interface area for the NR matrix to cross-link and interact with the filler. The monodispersed nanofillers can provide strong adhesion between the filler and NR matrix. The nanofiller-NR matrix interface can be engineered in such a way that the nanofiller provide optimum performance in reinforcement and enhancement in physicomachanical properties. Current trend in the nanofillers and overview of nanomaterials for the development of NRN are deliberated in the following sections.

### **2.5.1 Carbon Black**

Carbon black is a material produced by the incomplete combustion of heavy petroleum products. Carbon black is a form of paracrystalline carbon that has a high surface area to volume ratio. The carbon black is mainly used as the reinforcing filler in tires and other rubber products. It is also commonly used in the aerospace industry for the development of elastomers for aircraft vibration control components and engine mounts. Also carbon black improves the mechanical properties such as tensile strength and wear resistance of the NR. The 70 % of the carbon black produced is used in automobile tires. Likewise, carbon black helps to improve the thermal conductivity of the rubber used in tire and drives the heat away from the tread and belt area. This helps to increase the life of tire and reduce thermal damages. The carbon blacks have chemisorbed oxygen complexes including carboxylic, lactonic, phenolic, and quinonic groups on their surfaces which contribute to the volatile nature of the material. Based on various parameters such as particle size, surface area and activity, structure and porosity, the carbon blacks are categorized into various types. These parameters have direct influence on the properties of the rubber compound. Generally, the mechanical properties such as modulus and tensile properties are found to be increasing with decreasing particle size due to this, the NRN shows high viscosity, electrical conductivity, and abrasion resistance. The particle size of the carbon black material is directly proportional to the scorch resistance properties. The Mooney viscosity and modulus of the carbon black-NRN mainly depend on the loading and structure of the carbon black in natural rubber matrix. Carbon black-based fillers reinforce the rubber compound and lowering the

compound cost. The physicochemical interactions between the NR matrix and carbon black reinforces improve the NRN. Recent trends in NRNs show inquisitiveness to use carbon black-based hybrid fillers to improve the physicomechanical properties of the NRNs [29, 30].

Types of carbon black used in tires

Name	Abbrev.	ASTM design	Particle size (nm)	Tensile strength (MPa)	Relative laboratory abrasion	Relative road wear abrasion
Superabrasion furnace	SAF	N110	20–25	25.2	1.35	1.25
Intermediate SAF	ISAF	N220	24–33	23.1	1.25	1.15
High abrasion furnace	HAF	N330	28–36	22.4	1.00	1.00
Easy processing channel	EPC	N300	30–35	21.7	0.80	0.90
Fast extruding furnace	FEF	N550	39–55	18.2	0.64	0.72
High modulus furnace	HMF	N683	49–73	16.1	0.56	0.66
Semi-reinforcing furnace	SRF	N770	70–96	14.7	0.48	0.60
Fine thermal	FT	N880	180–200	12.6	0.22	–
Medium thermal	MT	N990	250–350	9.8	0.18	–

## 2.5.2 Clay

Montmorillonite (MMT)-, hectorite-, and rectorite-based natural clay fillers are attracting research interest due to their environmental friendly and non-polluting nature. MMT consists of the layered aluminosilicates stacked over one another. The interlayer distance between the aluminosilicates is in the order of 10–1000 nm [31]. Even though the electrostatic force between silicate layers limits the intercalation of clay-based fillers with the natural rubber matrix, they have been widely used as reinforcement material in the preparation of NRNs. Using various solvents, the interlayer spacing between the clay fillers can be expanded using a stepwise swelling process and improve the dispersion of the fillers. The concept of utilization of layered silicate fillers as reinforcing materials for the production of polymer nanocomposites was invented by Toyota research group. It is also to be considered that the physicochemical properties of clay fillers to exfoliate them and get good dispersion properties. The properties of the clay filler must be compatible with that of polymer and it must favor the steric repulsion of the chains to push the layers apart from each other. The strong interfacial interaction between the polymer and clay leads to the agglomeration due to the intercalation of clay fillers without the exfoliation of silicate layers and restricts the dispersion of fillers in the natural

rubber matrix. In order to overcome this issue, the clay fillers are modified by exchanging the interlayer cations with organic cations to increase the organophilic properties and make them compatible with the natural rubber [32]. The exfoliated layers in the clay fillers provide unique characteristics for interfacial intercalation of natural rubber polymer chain which result the enhancement in reinforcement properties.

### 2.5.3 Carbon Nanotubes

Carbon nanotubes (CNTs) were discovered by Sumio Iijima in 1991. The  $sp^2$  hybridized carbon atoms present in the CNT-based fillers provide unique electrical and thermal conductivity to the NRNs. The physicochemical properties of the CNTs are influenced by the chirality and diameter of the carbon nanotubes. The CNTs are classified into two types as single-walled nanotubes and multiwalled nanotubes. The CNTs are generally used as reinforcing agents for high-performance rubber composites due to their high mechanical, thermal, electrical, and physical properties. NRNs of the CNTs can be prepared by solution mixing. Due to the low dispersion of CNTs in the polymer matrix, variety of methods are adopted to make CNT-NRNs. This method includes solution mixing in which the dispersion of CNTs mixed with monomer solution followed by polymerization of the monomers, dispersion of CNTs and dispersion of polymers are added together in a solvent followed by the removal of solvent by evaporation, and dispersed nanotubes are added to dispersed monomer followed by polymerization, etc. Melt mixing is a common and simple method, particularly useful for polymers like rubber. In melt processing, CNTs are mechanically dispersed into the natural rubber matrix using a high-temperature and high-shear force mixer or compounder. The shear forces help to break nanotube aggregates or prevent their formation. The disadvantage of this method is that the dispersion of CNTs in the rubber matrix is quite poor compared to the dispersion that may be achieved through solution mixing.

In addition, the CNTs must be lower due to the high viscosities of the composites at higher loading of CNTs. In the in situ polymerization method, the CNTs are dispersed in monomer followed by polymerization. A higher percentage of CNTs may be easily dispersed in this method and form a strong interaction with the natural rubber matrix. The high viscosity of the natural rubber inhibits the dispersion of CNTs with high aspect ratio into the natural rubber matrix. In order to achieve desired physicomechanical properties, we have to introduce some pre-treatment techniques to functionalize the CNT fillers before compositing process. The conductivity of the rubber material can be improved by adding CNT fillers. The presence of CNT fillers in natural rubber matrix can be detected by Raman spectroscopic technique [33, 34]. The surface functionalization techniques are used to improve the dispersion of the CNTs. It can be classified into covalent and non-covalent functionalization. In the non-covalent functionalization, the ionic attachment of functional groups by neutralization of the acid-modified CNTs is

performed by using metal oxides. As a result of these ionic attachments, ionic clusters are formed which inhibit the separation of the carbon nanotubes. Due to this reason, normally covalent functionalization is advisable for the preparation of CNT-NRN to avoid the inter particle attraction between the CNTs [35]. For the bulk production of CNT-NRN, different methods including spray drying and two-roll mill assisted solvent mixing are adopted [36].

#### 2.5.4 Iron Oxide

Ferromagnetic  $\alpha$ -Fe<sub>2</sub>O<sub>3</sub> materials are economically viable, non-toxic, and thermodynamically stable nanomaterials which can be used as filler material for reinforcement and enhancing magnetic properties of NRNs.  $\alpha$ -Fe<sub>2</sub>O<sub>3</sub> is also called as hematite. Hematite nanomaterials have been studied for the wide range of applications because their magnetic properties greatly depend on their size and shape. The magnetic properties of  $\alpha$ -Fe<sub>2</sub>O<sub>3</sub> nanoparticles are of different shapes (spherical, rhombohedral, and circular) and can be prepared as powders by a various methods [37]. Ferromagnetic materials have different electrical, magnetic, electro-optical, and chemical properties depending on the different size variations in the nanometer range (1–100 nm). The nanomagnetic materials are characterized by different structural length scale, ranging from few interatomic distances to one micron. The magnetic moment  $m$ , in the nanomaterials, is originated from partially filled electrons in the inner shell of transition and rare earth materials. The magnetic moments are from the contribution of both spin  $S$  and orbital's  $L$ . Magnetic NRNs are having great research interest in the field of development of magnetic data storage media, drug delivery, magnetic sensors, actuators, etc. [38–41]. The magnetic-natural rubber nanoblends are prepared by mixing iron oxide nanoparticles with the natural rubber matrix followed by vulcanization process [42, 43].

The desired ferromagnetic properties can be imparted to the NRN by mixing the iron oxide nanofillers with specific size and magnetic properties. The elastomeric iron oxide-NRN can be used for flexible application platform for high voltage alternating current applications [44–46]. The magnetic and electrical properties of nanostructured iron oxide particles depends on the size of the nanoparticles. So by tuning the size of the iron oxide fillers, particular magnetic properties can be achieved [47–51]. (Ni-Fe<sub>2</sub>O<sub>3</sub>-NR) Jong-Ryul Jeong et al. (2004) synthesized  $\gamma$ -Fe<sub>2</sub>O<sub>3</sub> nanoparticles using chemical coprecipitation technique through a typical pipette drop method (pipette diameter: 2000  $\mu$ m) and a piezoelectric nozzle method (nozzle size: 50  $\mu$ m). The size distribution of the  $\gamma$ -Fe<sub>2</sub>O<sub>3</sub> nanoparticles prepared by the pipette drop method is from 5 to 8 nm. However, the nanoparticles made by the piezoelectric nozzle method show smaller and very narrow size distribution from 3 to 5 nm. Zero-field-cooled (ZFC)/field-cooled (FC) magnetization and magnetic hysteresis measurements were performed using superconducting quantum interference device (SQUID) magnetometer from 5 to 300 K to investigate the magnetic properties of the nanoparticles. The SQUID measurements revealed that the

superparamagnetism of nanoparticles with the blocking temperature of 119.5 and 94.3 K for the nanoparticles made by the pipette drop method and the piezoelectric nozzle method, respectively.

### 2.5.5 Zinc Oxide

Zinc oxide (ZnO) is a white inorganic powder. It is nearly insoluble in water but soluble in acids or alkalies. ZnO is often called as II–VI semiconductor because zinc and oxygen belong to the 2nd and 6th groups of the periodic table, respectively. ZnO has a wide band gap (3.37 eV) and a large exciton binding energy (60 meV) and exhibits many potential applications in areas such as laser diodes, solar cells, gas sensors, optoelectronic devices, and rubber technology. ZnO has three crystal forms: the hexagonal wurtzite, the cubic zinc blende, and the cubic rock salt which is rarely observed. The wurtzite structure is the most commonly used as it has the highest stability under normal working conditions. Hexagonal and zinc blende structures do not display inversion symmetry and its properties are responsible for the piezoelectricity and pyroelectricity of ZnO. This semiconductor material has several favorable features such as: good transparency, high electron mobility, wide band gap, and strong room temperature luminescence. ZnO is widely used in rubber industry as curing agent and activator for sulfur vulcanization [52]. The surface adsorption of accelerators, sulfur, and fatty acids in natural rubber matrix on the ZnO nanoparticles assists in the formation of intermediate complexes which solubilizes the insoluble accelerators to form the catalyst which enhances the vulcanization process and cure characteristics of the NRNs [53, 54]. The nanosized zinc oxide can easily form hydroxyl complexes over the surface act as template for the formation of reactive intermediates which improves the dynamics of vulcanization reaction (Fig. 2.29).

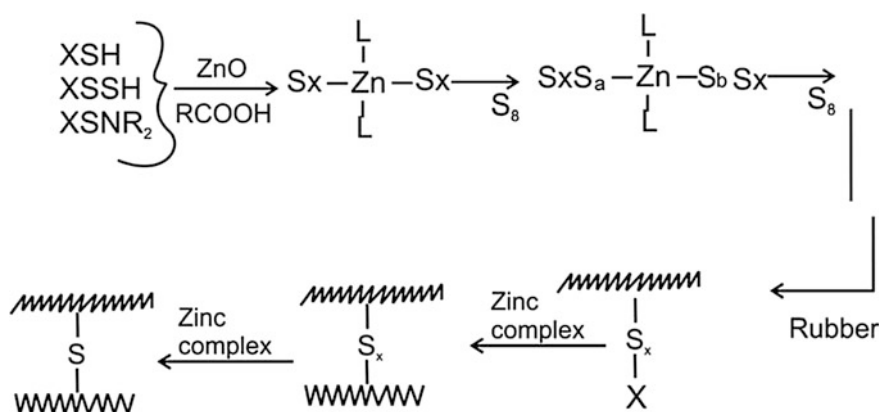


**Fig. 2.29** Schematic showing the role of ZnO and fatty acid in accelerated sulfur vulcanization (X-accelerator residue, L-ligand)

The optimal concentration required for the catalytic conversion of accelerator to the zinc–accelerator sulfur complex was identified by Duchacek [52]. It is found that the optimum zinc oxide content to minimize reversion was slightly greater than this minimum. The high surface to volume ratio of nanosized ZnO provides high surface interface area, for chemisorption of accelerator molecules enhances the chemical kinetics of vulcanization reaction by increasing the formation of intermediate efficiency of accelerator–zinc complex [56]. Zinc oxide nanoparticles help to increase the cross-linking ability of monomers to form natural rubber matrix. ZnO nanoparticles act as sulfur transporting agent to include the sulfur atoms into the hydrocarbon chains. The ZnO nanoparticle-based fillers show better physico-mechanical property than the conventional bulk ZnO nanofillers. It also helps to improve the reinforcing index, flex resistance, cross-linking density, and tensile properties of the NRNs [57].

### 2.5.6 *Nickel*

Nickel metal nanoparticles are used as magnetic fillers in natural rubber to incorporate the magnetic properties of nickel nanoparticles to the elastomeric composite of natural rubber. The electrical conductivity of the NRN increases with nickel loading concentration. Girgis et al. observed that the optimal loading concentration of 30 phr of nickel provides better rheological and electrical properties compared to that of iron [58]. M.R. Anantharaman et al. observed that the nickel nanoparticle can change the dielectric and magnetic properties of rubber simultaneously. The natural rubber–nickel nanocomposites can be used as flexible magnetic shielding materials for safety applications. The nanoengineered elastomers of nickel metal nanoparticles can be used for application in fabrication of low-frequency electronic peripherals. The dielectric permittivity of nickel-NRNs can be tuned by controlling the loading of nickel metal nanoparticles in the natural rubber matrix. The elastic modulus and magnetic properties of the nickel-NRN were proportional to the weight percentage loading of nickel nanoparticles in the rubber matrix. The dielectric permittivity of nickel-rubber nanocomposite was inversely proportional to the temperature, and the heterogeneous nature of the composite material attributes an interfacial polarization which results a change in dielectric permittivity with frequency as well as filler concentration. It is observed that the high volume expansion of elastomeric rubber indulges the dielectric permittivity of the nickel-loaded NRNs [59].

### 2.5.7 *Silica*

Monodisperse silica ( $\text{SiO}_2$ ) is a promising alternative for carbon black, which invites industrial attention due to its light color and glossy nature. It is well

acknowledged that the rolling resistance of tire can be improved by adding  $\text{SiO}_2$  nanofillers. The hydrophilic and polar nature of silica is not compatible with the apolar polymer matrix like natural rubber. Due to this discordancy between silica filler and natural rubber matrix, the surface functionalization of silica is inevitable for the better intercalation of natural rubber matrix with silica filler [60]. Sol-gel technique is commonly used method to prepare nanostructured  $\text{SiO}_2$  particles. In sol-gel method, an alkoxy precursor of silicon is dissolved in an organic solvents like propanol or ethanol followed by the addition of slightly acidic catalyst to initiate the polymerization reaction by the polycondensation of water molecules to form  $\text{SiO}_2$  networks. The obtained gel was heated to remove the organic solvent to form silica xerogel. The xerogel was calcined above  $800^\circ\text{C}$  to obtain the  $\text{SiO}_2$  nanoparticles. Debapriya et al. observed that during the in situ polymerization of silica in natural rubber matrix, the cross-linking density of rubber composite increases with the loading of  $\text{SiO}_2$  [61] (Fig. 2.30).

R. Scotti et al. demonstrated that the alkylthiol and alkyl polysulfide functionalized silica form anisotropic silica fillers which provide better interfacial surface interaction between silica fillers and rubber polymer matrix. The surface functionalization using thiol and polysulfide groups provides enhancement in filler–filler interaction and filler–natural rubber polymer matrix interaction due to their ability in inducing in situ formation of anisotropic  $\text{SiO}_2$  [62]. S. Chuayjuljit et al. observed that the differential microemulsion polymerization technique can be adopted for the synthesis of NRN using polystyrene coated silica nanoparticles. The study revealed

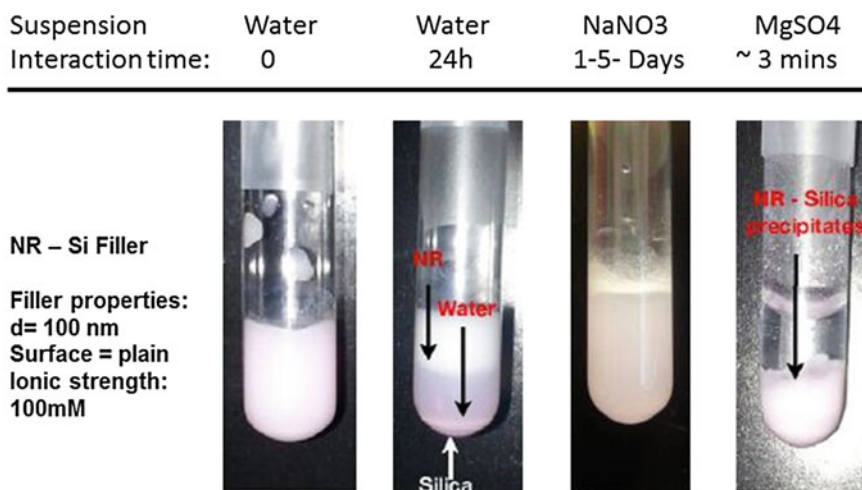


**Fig. 2.30** Photographs of the mixed solutions of NR-100 nm plain silica in water,  $\text{NaNO}_3$ , and  $\text{MgSO}_4$  suspension at 100 mM ionic strength. Aggregation was observed only in the presence of ions. Similar results can be obtained for NR-30-nm plain silica suspensions. NR concentration:  $\sim 0.7$  wt%; volume percent ratio (dry silica/dry NR): 20 %. “Adapted with permission from Chan AJ et al./Langmuir, 2015, 31 (45), 12437–12446.” Copyright (2014) American Chemical Society

that the optimized amount of polystyrene coated silica fillers reinforces the physicochemical properties of the NRN. The prepared NRN exhibited excellent tensile strength, improved elasticity of rubber molecules near the glass transition temperature values and flammability due to the enriched mechanical and functional properties [63]. Nanosilica fillers also help to achieve better cure characteristics and tear strength through the interfacial interaction between filler and rubber matrix [64].

### 2.5.8 Graphene

Single-layer graphene is a purely two-dimensional material. Its lattice consists of regular hexagons with a carbon atom at each corner. The bond length between the adjacent carbon atoms is  $1.42 \text{ \AA}$  and the lattice constant,  $a$ , is  $2.46 \text{ \AA}$  (Fig. 2.31). The first report on this material appeared several decades ago, even before the name graphene had been coined, but it took the pioneering work done by the Manchester research group in 2004 to spark the present explosion of interest in this material [65]. At present, the most popular approaches for the graphene preparation are mechanical exfoliation, growth on metals, and subsequent graphene transfer to insulating substrates, and thermal decomposition of SiC to produce so-called epitaxial graphene on top of SiC wafers. Exfoliation is the most popular for laboratory use, and it is well suited for the fabrication of graphene-NRNs due to their feasibility in solution-based vulcanization processes. The delocalized electrons present in the graphene network give electrical conductivity to this material in addition to the in-plane  $\sigma$  C–C bond which provides extraordinary mechanical stability and strength. Graphene-based nanofillers and reinforcing agents provide large surface

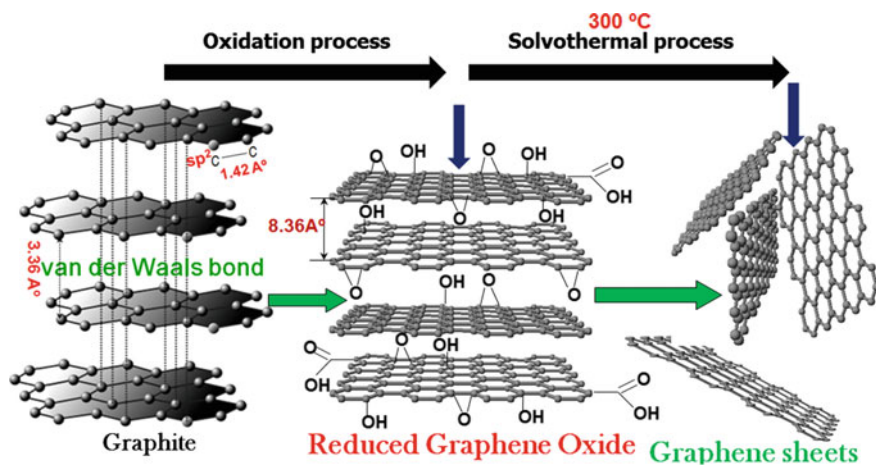


Fig. 2.31 Schematic of solvothermal formation of graphene sheets

interface interaction between graphene and rubber polymer matrix, and it also facilitates the intercalation of natural rubber matrix with the two-dimensional network of carbon atoms. These strong interfacial interactions make them mechanically stable and highly flexible without losing the electrical and electronic conductivity which is preferred for the development of NRNs for the flexible electronics applications.

### ***2.5.9 Gold and Silver Metal Nanoparticles***

Gold nanoparticles (GNPs) are generally purple pink color, and the color is tuned by varying the size of the Au nanoparticles. GNPs are generally prepared by reducing gold precursors through solution process. Surface plasmon resonance and size-dependent photoluminescent properties of nanosized gold particles are of particular interest due to their huge potential in membrane-based sensors. The Au nanoparticle-incorporated flexible natural rubber composites can replace conventional sensor modules in analytical instruments. GNPs show an optical quenching upon change in the pH of the elastomer, it is found that the GNPs tend to agglomerate when the pH is changed and this agglomeration bases the reduction in surface plasmon resonance. The photoluminescent properties of natural rubber can be mainly attributed to the organic acid components of latex. The GNPs incorporated into the natural rubber matrix interact with these organic acid complexes which influence their photoluminescent properties. Job et al. demonstrated that the natural rubber can be used as a substrate to reduce the Au atoms present in the gold precursor materials and form GNPs. This in situ reduction process result the formation of metallic nanoclusters on the surface of natural rubber substrate [66].

Silver nanoparticles (SNPs) are considered for wide range of applications such as development of antimicrobial, electrical, thermal, and optical functional materials. SNPs have glossy faint greenish color with optical and electronic properties suitable for industrial applications. In comparison with the broad optical absorption band of natural rubber at 239 nm, SNPs have optical absorption band around 425 and 484 nm. SNPs also exhibit surface plasmon resonance, and the band gap of SNPs can be tuned by varying particle size. SNP is the only material with tunable surface plasmon resonance which can be regulated into any wavelength in the visible spectrum. The SNP-NRNs have huge potential in the development of flexible antimicrobial coatings, elastomeric optical transducers, flexible electronic components, and membrane-based sensors [67] (Fig. 2.32).

SNPs can be synthesized by adopting different methods such as chemical reduction, photoreduction, and microwave-assisted reduction process. The common methods used for the synthesis of silver nanoparticles include Turkevich method, Lee-Meisel method, and Creighton method [55, 68, 69]. In Turkevich method,  $\text{AgNO}_3$  is used as silver source and reduction of this metal source produces silver nanoparticles in a narrow distribution of particle sizes but in Meisel method, a broad range of silver nanoparticles can be produced through the chemical reduction

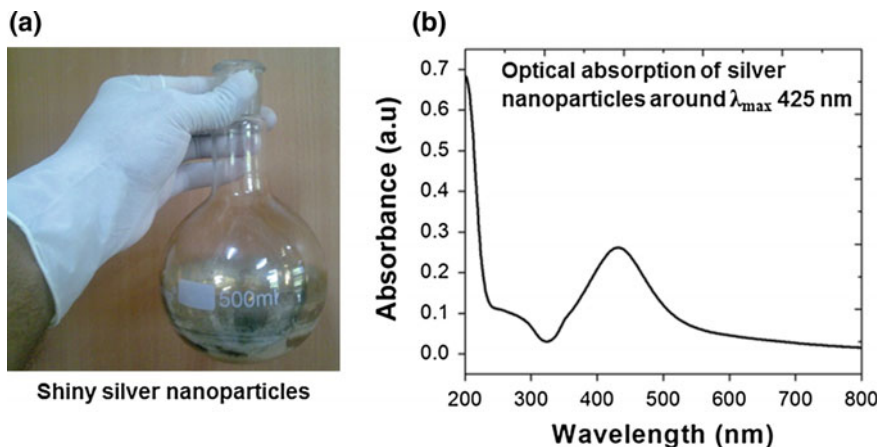


**Fig. 2.32** **a** Picture showing the silver nanoparticles coated inside the glass bottle 32, **b** UV–Vis absorption spectrum of silver nanoparticles

method. In Creighton method,  $\text{NaBH}_4$  is used as the reducing agent to reduce  $\text{AgNO}_3$  metal source, and the SNPs synthesized by this method have very narrow size distribution with 10 nm average particle size [56].

## 2.6 Summary and Outlook

In summary, this chapter provides an introduction to NRNs and various strategies for fabricating NRNs. A general out look of literature has been provided followed by the major outcomes of recent research trends. Different types and synthesis methods for preparing NRNs include skim latex mixing, latex/melt intercalation method, freeze-drying and in situ non-aqueous sol-gel method. It is followed by the schematic representations of various physicochemical characterization techniques including XRD, XPS, XRF, UV–Vis spectroscopy, photoluminescence spectroscopy, Raman spectroscopy, TGA-DTA, SEM-EDX, EPMA, TEM-SAED, VSM, and FTIR. Those techniques can be used for analyzing various composite properties such as structural, thermal, optical, morphological, magnetic, and size distribution of the constituent nanofillers. A brief idea of currently available novel nanofillers including iron oxide, carbon black, graphene, silver, and gold nanoparticles which are utilized for the successful development of NRNs was described. In addition, by changing the physicochemical properties of the nanofillers, the composite properties can be tuned with desired nanofunctionalities in order to employ them in various applications such as flexible electronic applications, antimicrobial coating, membrane-based sensors have been elaborately deliberated to get a clear notion.

## References

1. Bendahou A, Kaddami H, Dufresne A (2010) Investigation on the effect of cellulosic nanoparticles morphology on the properties of natural rubber based nanocomposites. *Eur Polymer J* 46:609–620
2. Jinrong W et al (2013) Vulcanization kinetics of graphene/natural rubber nanocomposites. *Polymer* 54:3314–3323
3. Suil G et al (2008) Preparation and properties of natural rubber composites reinforced with pretreated carbon nanotubes. *Polym Adv Technol* 19:1543–1549
4. Thomas PS et al (2012) Electrical properties of natural rubber nanocomposites: effect of 1-octadecanol functionalization of carbon nanotubes. *J Mater Sci* 47:3344–3349
5. Nakason C, Kaesaman A, Supasanthitikul P (2004) The grafting of maleic anhydride onto natural rubber. *Polym Testing* 23(1):35–41
6. Bokobza L (2012) Multiwall carbon nanotube-filled natural rubber: electrical and mechanical properties, *eXPRESS. Polym Lett* 6(3):213–223
7. Il-Jin K et al (2010) Effect of nano zinc oxide on the cure characteristics and mechanical properties of the silica-filled natural rubber/butadiene rubber compounds. *J Appl Polym Sci* 117:1535–1543
8. Abraham E et al (2013) Physicomechanical properties of nanocomposites based on cellulose nanofibre and natural rubber latex. *Cellulose* 20:417–427
9. Kumari P, Unnikrishnan G (2013) Thermal properties of compatibilized and filled natural rubber/acrylonitrile butadiene rubber blends. *J Therm Anal Calorim* 114:67–75
10. Ajesh KZ et al (2014) Rheological behaviour of clay incorporated natural rubber and chlorobutyl rubber nanocomposites. *RSC Adv* 4:58047–58058
11. Jamal EMA et al (2009) Synthesis of nickel–rubber nanocomposites and evaluation of their dielectric properties. *Mater Sci Eng B* 156:24–31
12. Flavio C et al (2014) Organic acids and protein compounds causing the photoluminescence properties of natural rubber membranes and the quenching phenomena from Au nanoparticle incorporation. *Luminescence* 29:1047–1052
13. Bakar NHHA, Ismail J, Bakar MA (2007) Synthesis and characterization of silver nanoparticles in natural rubber. *Mater Chem Phys* 104:276–283
14. Zakaria MZ, Ahmad SH (2013) Investigation on thermal conductivity and mechanical properties of thermoplastic natural rubber filled with alumina and boron carbide nanocomposites. *Energy Environ Eng J* 4(1):11–14
15. Dong-Ah L et al (2012) Natural rubber/fluoroelastomer blended composites using colloid stabilization-destabilization method. *Macromol Res* 20(7):673–681
16. Kaltseis R et al (2014) Natural rubber for sustainable high-power electrical energy generation. *RSC Adv* 4:27905
17. Quitmann D et al (2013) Solvent-sensitive reversible stress-response of shape memory natural rubber. *ACS Appl Mater Interfaces* 5:3504–3507
18. Venkatanarasimhan S, Raghavachari D (2013) Epoxidized natural rubber–magnetite nanocomposites for oil spill recovery. *J Mater Chem A* 1:868
19. Chen Y, Yuan D, Xu C (2014) Dynamically vulcanized biobased polylactide/natural rubber blend material with continuous cross-linked rubber phase. *ACS Appl Mater Interfaces* 6:3811–3816
20. Parulekar Y, Mohanty AK (2006) Biodegradable toughened polymers from renewable resources: blends of polyhydroxybutyrate with epoxidized natural rubber and maleated polybutadiene. *Green Chem* 8:206–213
21. Kong I et al (2010) Magnetic and microwave absorbing properties of magnetite–thermoplastic natural rubber nanocomposites. *J Magn Magn Mater* 322:3401–3409
22. Sookyung U et al (2014) Influence of modifying agents of organoclay on properties of nanocomposites based on natural rubber. *Polym Testing* 33:48–56

23. Hernandez M et al (2012) Overall performance of natural rubber/graphene nanocomposites. *Compos Sci Technol* 73:40–46
24. Potts JR et al (2012) Processing–morphology–property relationships and composite theory analysis of reduced graphene oxide/natural rubber nanocomposites. *Macromolecules* 45:6045–6055
25. Alex R, Nah C (2006) Preparation and characterization of organoclay-rubber nanocomposites via a new route with skim natural rubber latex. *J Appl Polym Sci* 102:3277–3285
26. Abdollahi M et al (2011) Structure and properties of natural rubber/butadiene rubber (NR/BR) blend/sodium montmorillonite nanocomposites prepared via a combined latex/melt intercalation method. *Polym Sci Ser A* 53(12):1175–1181
27. Pojanavaraphan T, Magaraphan R (2008) Prevulcanized natural rubber latex/clay aerogel nanocomposites. *Eur Polym J* 44:1968–1977
28. Wahba L et al (2014) A novel non-aqueous sol–gel route for the *in situ* synthesis of high loaded silica–rubber nanocomposites. *Soft Matter* 10:2234–2244
29. Thapong P et al (2014) Properties of natural rubber reinforced by carbon black-based hybrid fillers. *Polym-Plast Technol Eng* 53(8):818–823
30. Bhattacharya M, Bhowmick AK (2010) Synergy in carbon black-filled natural rubber nanocomposites Part I: mechanical, dynamic mechanical properties and morphology. *J Mater Sci* 45:6126–6138
31. Mondragon M et al (2009) Injection molded thermoplastic starch/natural rubber/clay nanocomposites: morphology and mechanical properties. *Carbohydr Polym* 77:80–86
32. Rezende CA et al (2010) Natural rubber-clay nanocomposites: mechanical and structural properties. *Polymer* 51:3644–3652
33. Kueseng K, Jacob KI (2006) Natural rubber nanocomposites with SiC nanoparticles and carbon nanotubes. *Eur Polymer J* 42:220–227
34. Kueseng P, Sae-oui P, Rattanasom N (2013) Mechanical and electrical properties of natural rubber and nitrile rubber blends filled with multi-wall carbon nanotube: effect of preparation methods. *Polym Testing* 32:731–738
35. Sui G et al (2008) Preparation and properties of natural rubber composites reinforced with pretreated carbon nanotubes. *Polym Adv Technol* 19:1543–1549
36. Thomas PS et al (2012) Electrical properties of natural rubber nanocomposites: effect of 1-octadecanol functionalization of carbon nanotubes. *J Mater Sci* 47:3344–3349
37. Zhang X et al (2013) Synthesis, optical and magnetic properties of  $\alpha$ -Fe<sub>2</sub>O<sub>3</sub> nanoparticles with various shapes. *Mater Lett* 99:111–114
38. Qiaoling LI, Zhang C (2010) Preparation of Fe<sub>2</sub>O<sub>3</sub> microtubules and the effect of a surfactant on their properties. *J Ceram Process Res* 11(3):331–334
39. Chirita M, Grozescu I (2009) Fe<sub>2</sub>O<sub>3</sub>—nanoparticles, physical properties and their photochemical and photoelectrochemical applications. *Chem bull “POLITEHNICA” Univ (Timisoara)* 54(68): 1–8
40. Jong-Ryul J et al (2004) Magnetic properties of  $\gamma$ -Fe<sub>2</sub>O<sub>3</sub> nanoparticles made by coprecipitation method. *Phys Status Solidi (b)* 241(7):1593–1596
41. Suber L et al (1998) Structural and magnetic properties of  $\alpha$ -Fe<sub>2</sub>O<sub>3</sub> nanoparticles. *Appl Organomet Chem* 12:347–351
42. Akbar S et al (2004) Synthesis of Fe<sub>2</sub>O<sub>3</sub> nanoparticles by new Sol-Gel method and their structural and magnetic characterizations. *Ar Xiv:cond-mat/0408480*
43. Teng X, Yang H (2004) Effects of surfactants and synthetic conditions on the sizes and self-assembly of monodisperse iron oxide nanoparticles. *J Mater Chem* 14:774–779
44. Sahoo SK et al (2010) Characterization of  $\gamma$ - and  $\alpha$ -Fe<sub>2</sub>O<sub>3</sub> nano powders synthesized by emulsion precipitation-calcination route and rheological behaviour of  $\alpha$ -Fe<sub>2</sub>O<sub>3</sub>. *Int J Eng Sci Technol* 2(8):118–126
45. Ma J et al (2010)  $\alpha$ -Fe<sub>2</sub>O<sub>3</sub>: hydrothermal synthesis, magnetic and electrochemical properties. *J Phys Chem C* 114(24):10671–10676
46. Liu L et al (2006) Surfactant-assisted synthesis of  $\alpha$ -Fe<sub>2</sub>O<sub>3</sub> nanotubes and nanorods with shape-dependent magnetic properties. *J Phys Chem B* 110(31):15218–15223

47. Wu C et al (2006) Synthesis of hematite ( $\alpha$ -Fe<sub>2</sub>O<sub>3</sub>) nanorods: diameter-size and shape effects on their applications in magnetism, lithium ion battery, and gas sensors. *J Phys Chem B* 110 (36):17806–17812
48. Liao L et al (2008) Morphology controllable synthesis of  $\alpha$ -Fe<sub>2</sub>O<sub>3</sub> 1D nanostructures: growth mechanism and nano device based on single nanowire. *J Phys Chem C* 112(29):10784–10788
49. Wang X et al (2009) Fast preparation, characterization, and property study of  $\alpha$ -Fe<sub>2</sub>O<sub>3</sub> nanoparticles via a simple solution-combusting method. *J Phys Chem C* 113(17):7003–7008
50. Cao SW, Zhu YJ (2008) Hierarchically nanostructured  $\alpha$ -Fe<sub>2</sub>O<sub>3</sub> hollow spheres: preparation, growth mechanism, photocatalytic property, and application in water treatment. *J Phys Chem C* 112(16):6253–6257
51. El-Nashar DE, Mansour SH, Girgis E (2006) Nickel and iron nano-particles in natural rubber composites. *J Mater Sci* 41:5359–5364
52. Duchacek V (1978) Effect of thiourea on thiuram-accelerated sulfur vulcanization and its significance for vulcanization mechanism. *J Appl Polym Sci* 22(1):227–237
53. Barnard D et al (1970) Rubber natural. *Encyclopedia of polymer science and technology: plastics, resins, rubbers, fibers* 12:178
54. Sahoo S et al (2008) Synthetic zinc oxide nanoparticles as curing agent for polychloroprene. *Polym Polym Compos* 16(3):193–198
55. Lee PC, Meisel DJ (1982) Adsorption and surface-enhanced Raman of dyes on silver and gold sols. *J Phys Chem* 86:3391–3395
56. Creighton JA, Blatchford CG, Albrecht MG (1979) Plasma resonance enhancement of Raman scattering by pyridine adsorbed on silver or gold sol particles of size comparable to the excitation wavelength. *J Chem Soc Farad Trans II* 75:790–798
57. Sabura BPM (2010) Studies on the use of nano zinc oxide and modified silica in NR, CR and SBR. <http://hdl.handle.net/10603/1406>
58. El-Nashar DE, Mansour SH, Girgis E (2006) Nickel and iron nano-particles in natural rubber composites. *J Mater Sci* 41:5359–5364
59. Jamal EMA et al (2009) Synthesis of nickel–rubber nanocomposites and evaluation of their dielectric properties. *Mater Sci Eng B* 156:24–31
60. Sarkawi SS et al (2013) Morphology of silica reinforced natural rubber: the effect of silane coupling agent. Presented at the fall 184th technical meeting of the rubber division of the American Chemical Society, inc. Cleveland, Ohio, 7–10 Oct. ISSN 1547-1977
61. Debapriya D et al (2014) Effect of sol-gel-derived nano-silica on the properties of natural rubber-poly butadiene rubber-reclaim rubber ternary blends/silica nanocomposites. *Polym-Plast Technol Eng* 53:1131–1141
62. Scotti R et al (2012) Rubber–silica nanocomposites obtained by in situ sol–gel method: particle shape influence on the filler–filler and filler–rubber interactions. *Soft Matter* 8:2131–2143
63. Chuayjuljit S, Boonmahithisud A (2010) Natural rubber nanocomposites using polystyrene-encapsulated nanosilica prepared by differential microemulsion polymerization. *Appl Surf Sci* 256:7211–7216
64. Lay M et al (2013) Effect of nanosilica fillers on the cure characteristics and mechanical properties of natural rubber composites. *Adv Mater Res* 626:818–822
65. Novoselov KS et al (2004) Electric field effect in atomically thin carbon films. *Science* 306:666–669
66. Flavio C et al (2014) Organic acids and protein compounds causing the photoluminescence properties of natural rubber membranes and the quenching phenomena from Au nanoparticle incorporation. *Luminescence* 29:1047–1052
67. BakarNHH Abu, Ismail J, Abu Bakar M (2007) Synthesis and characterization of silver nanoparticles in natural rubber. *Mater Chem Phys* 104:276–283
68. Turkevich J, Stevenson PC, Hillier J (1951) A study of the nucleation and growth processes in the synthesis of colloidal gold. *Disc Faraday Soc* 11:55–75
69. Lee PC, Meisel DJ (1982) Adsorption and surface-enhanced Raman of dyes on silver and gold sols. *Phys Chem* 86:3391–3395

Rubber Nano Blends

Preparation, Characterization and Applications

Markovic, G.; Visakh, P.M. (Eds.)

2017, VI, 349 p. 212 illus., 76 illus. in color., Hardcover

ISBN: 978-3-319-48718-2